

ECE 536 – Integrated Optics and Optoelectronics
Lecture 28 – April 28, 2022

Spring 2022

Tu-Th 11:00am-12:20pm

Prof. Umberto Ravaioli

ECE Department, University of Illinois

Lecture 28 Outline

- End Modulators
- Brief Review of Photodetectors

Acousto-optic Modulator

Acousto-optic Modulators

Also acousto-optic modulators control transmission of light by local changes of index of refraction in the medium.

- the modulation occurs by means of a travelling sound wave which induces a stress-related modification of the local index
- acoustic interactions travel at the speed of sound in the material, while electro-optic interactions can occur at nearly the speed of light
- while electro-optic interactions can be established with DC fields, acousto-optic modulation based on sound waves always involves interaction with travelling or standing waves in the solid

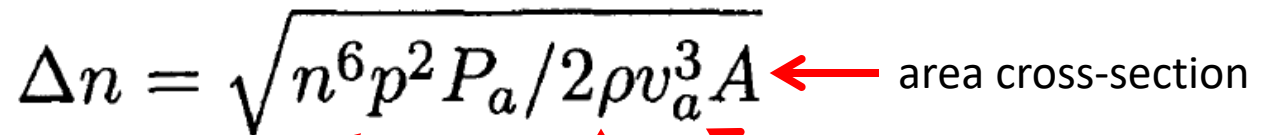
Acousto-optic Modulators

The photoelastic effect involves reflecting light due to the change of the index of refraction in a dielectric caused by strain. This effect is nonlinear and characterized by the fourth rank **photoelastic tensor** p_{ijkl}

term of the index ellipsoid $\Delta \left(\frac{1}{n^2} \right)_{ij} = p_{ijkl} S_{kl}$

strain $S_{kl}(r) = \frac{1}{2} \left[\frac{\partial u_k(r)}{\partial x_l} + \frac{\partial u_l(r)}{\partial x_k} \right]$

The acousto-optic strain interacts with an electric field component E_j to generate a polarization ΔP_i . The acoustic power P_a is related to the change in index of refraction through the relation

$$\Delta n = \sqrt{n^6 p^2 P_a / 2 \rho v_a^3 A}$$
The equation is $\Delta n = \sqrt{n^6 p^2 P_a / 2 \rho v_a^3 A}$. Red arrows point from labels below to terms in the equation: one from 'photoelastic tensor element' to p^2 , one from 'mass density' to ρ , one from 'acoustic velocity' to v_a^3 , and one from 'area cross-section' to A .

photoelastic tensor element

mass density

acoustic velocity

Acousto-optic Modulators

Rewriting in terms of a figure of merit $M = n^6 p^2 / \rho v_a^3$

$$\Delta n = \sqrt{M P_a / 2A}$$

Materials commonly used in Acousto-optic Modulators

<i>Materials</i>	$\lambda(\mu\text{m})$	n	$\rho(\text{g}/\text{cm}^3)$	$v_s(10^3 \text{ m/s})$	M
Fused Quartz	0.63	1.46	2.2	5.95	1.51×10^{-15}
GaAs	1.15	3.37	5.34	5.15	104×10^{-15}
LiNbO ₃	0.63	2.20	4.7	6.57	6.99×10^{-15}
YAG	0.63	1.83	4.2	8.53	0.012×10^{-15}
As ₂ S ₃	1.15	2.46	3.20	2.6	433×10^{-15}
PbMO ₄	0.63	2.4		3.75	73×10^{-15}

A good (old) reference on photoelastic tensor:

J. F. Nye, *Physical Properties of Crystals*, Oxford Clarendon Press, London, pp. 241 (1957)

Acousto-optic Modulators

Acousto-optic modulators used in integrated optics generally use travelling wave acoustic fields. The acoustic field creates a grating structure which can diffract the incident optical field.

Optical wave interaction can be produced by either bulk acoustic waves travelling in the volume of the material, or by surface acoustic waves (SAW) which propagate on the surface within approximately one acoustic wavelength of the surface.

SAW devices are well suited to integrated optics applications, because the energy of the acoustic field is concentrated in the region of the optical waveguide.

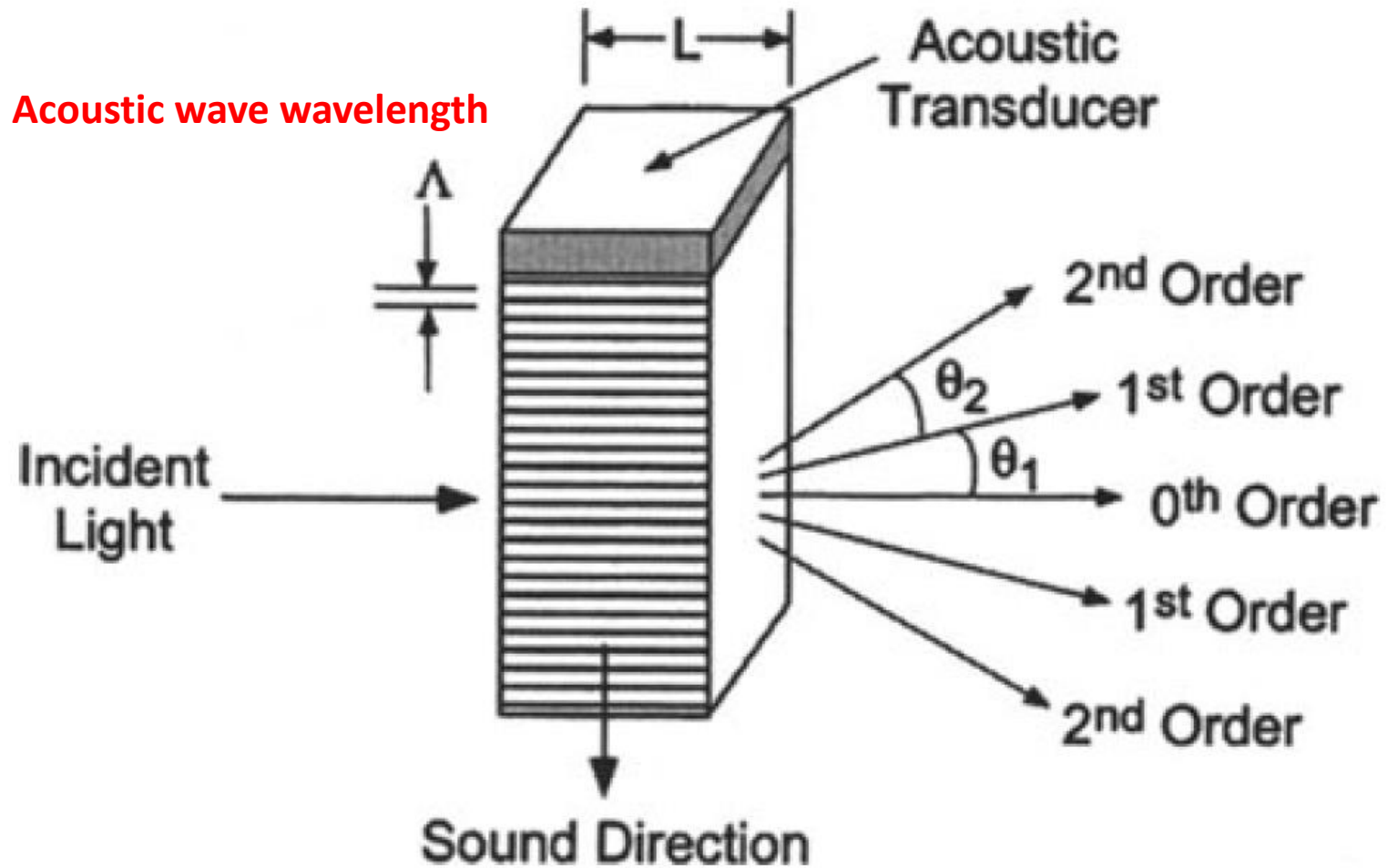
Diffraction in Acoustic Grating

Acusto-optic interaction can be described as a diffraction of an optical wave by a travelling phase grating induced by an acoustic wave.

As the phase grating Doppler-shifts the optical frequency, it can be used to deflect, modulate, or filter the optical beam.

Isotropic acusto-optic interactions which do not change the polarization of the optical beam can result in either multiple or single diffracted optical orders.

Acousto-optic Modulators



Acousto-optic Modulators

There are two basic configurations:

If the optical field propagates transverse to the acoustic beam, and the interaction length of the two beams is relatively short we have **Raman-Nath** diffraction

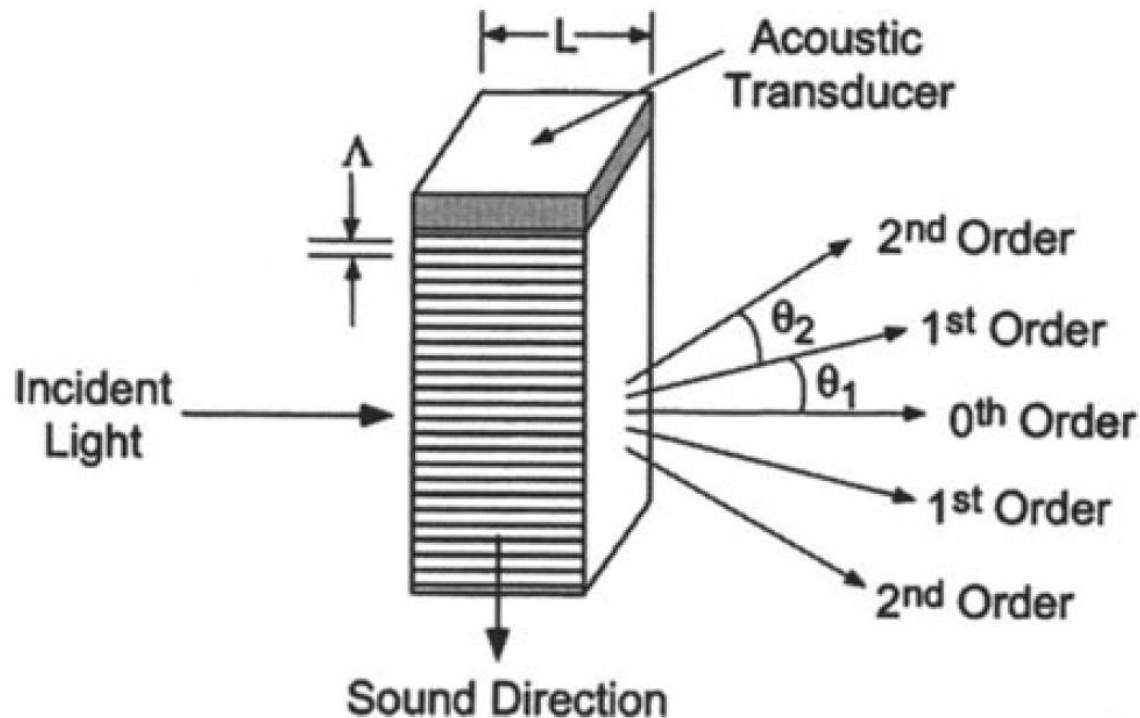
$$L \ll \frac{\Lambda^2}{(\lambda/n)}$$

If the acoustic field is large so that **multiple refraction** can occur, the interaction is called **Bragg** modulation.

$$L \gg \frac{\Lambda^2}{(\lambda/n)}$$

Raman-Nath Diffraction Regime

The Raman-Nath regime is observed at relatively low acoustic frequencies at small acousto-optic interaction lengths. This type of diffraction takes place at an arbitrary incident angle of light roughly normal to the acoustic beam and the diffraction pattern contains many diffraction orders of symmetrically distributed light intensity (which can be studied with Bessel functions).



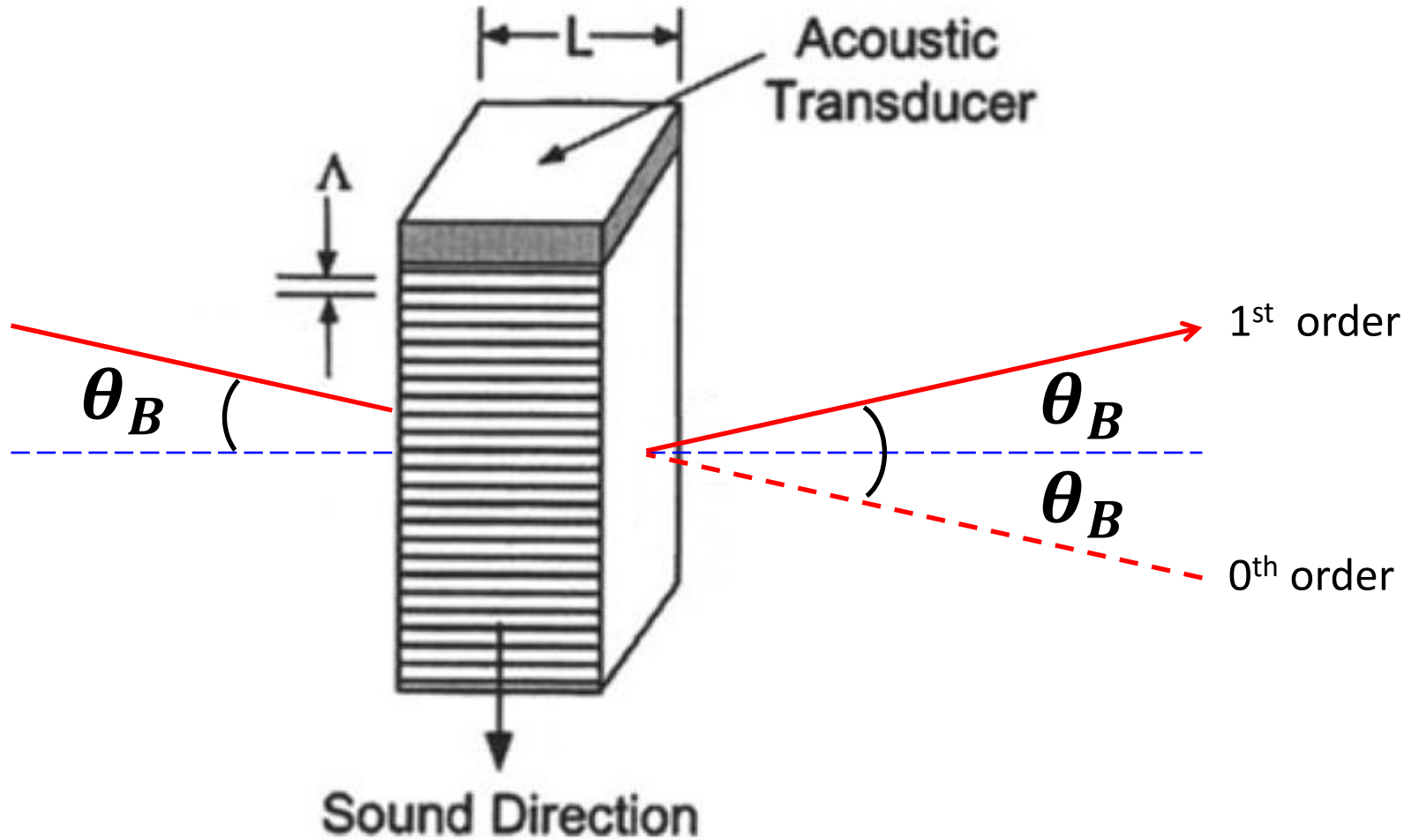
Bragg Diffraction Regime

By contrast, the Bragg regime is observed at high acoustic frequencies usually exceeding 100MHz . The diffraction pattern of this regime even at large acoustic power consists of two diffraction maxima of zero and first orders.

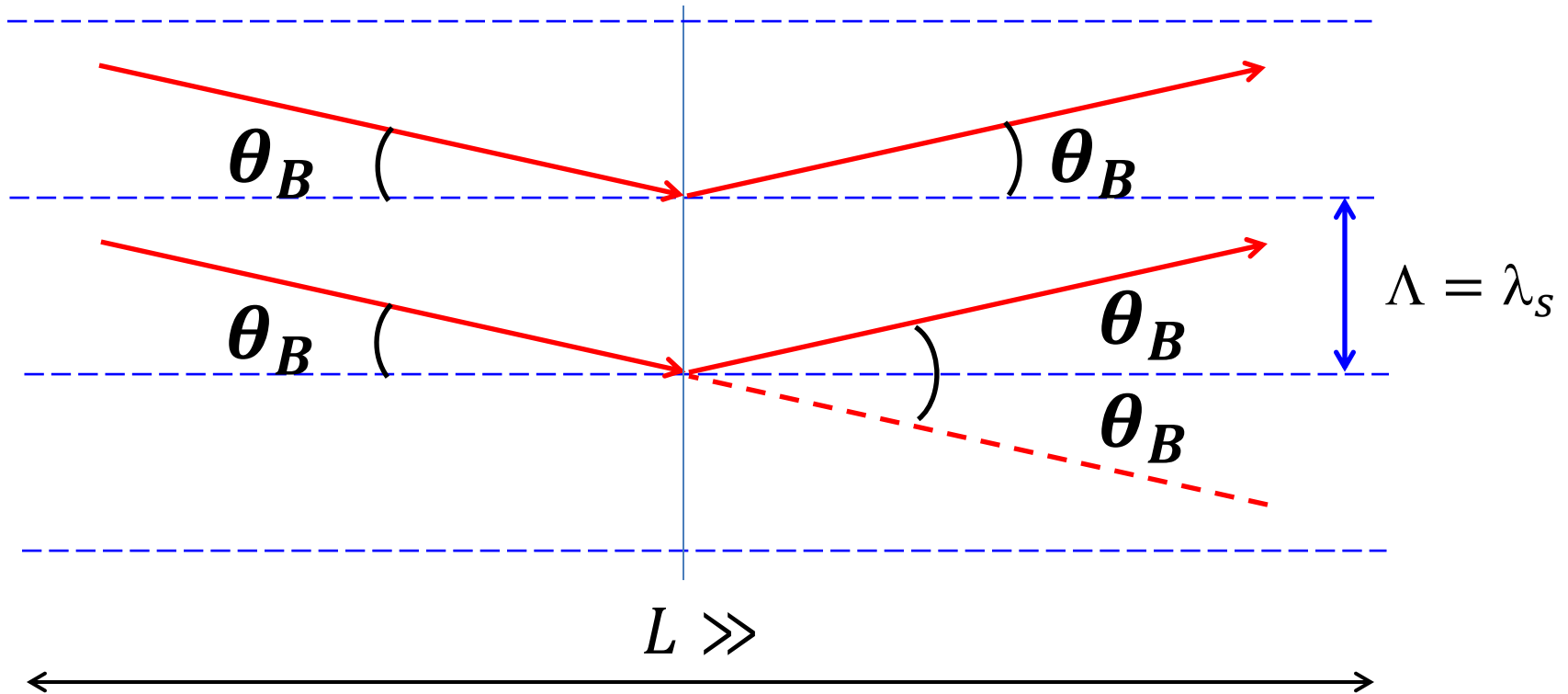
At the Bragg angle of incidence θ_B only one diffraction order is produced while others are annihilated by destructive interference.

This single-order isotropic Bragg diffraction is much more efficient and therefore is widely used in practical devices.

Bragg Diffraction Regime



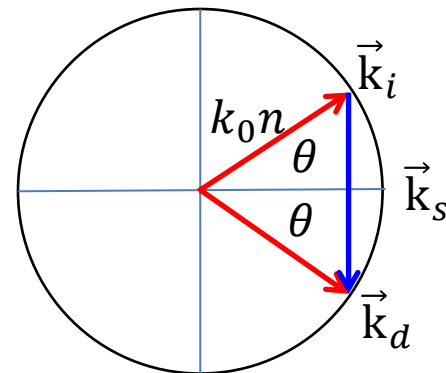
Bragg Diffraction Regime



$$2k_0 n \sin \theta_B = k_s$$

$$2 \frac{2\pi}{\lambda_0} n \sin \theta_B = \frac{2\pi}{\Lambda}$$

$$2\Lambda \sin \theta_B = \lambda_0 / n$$

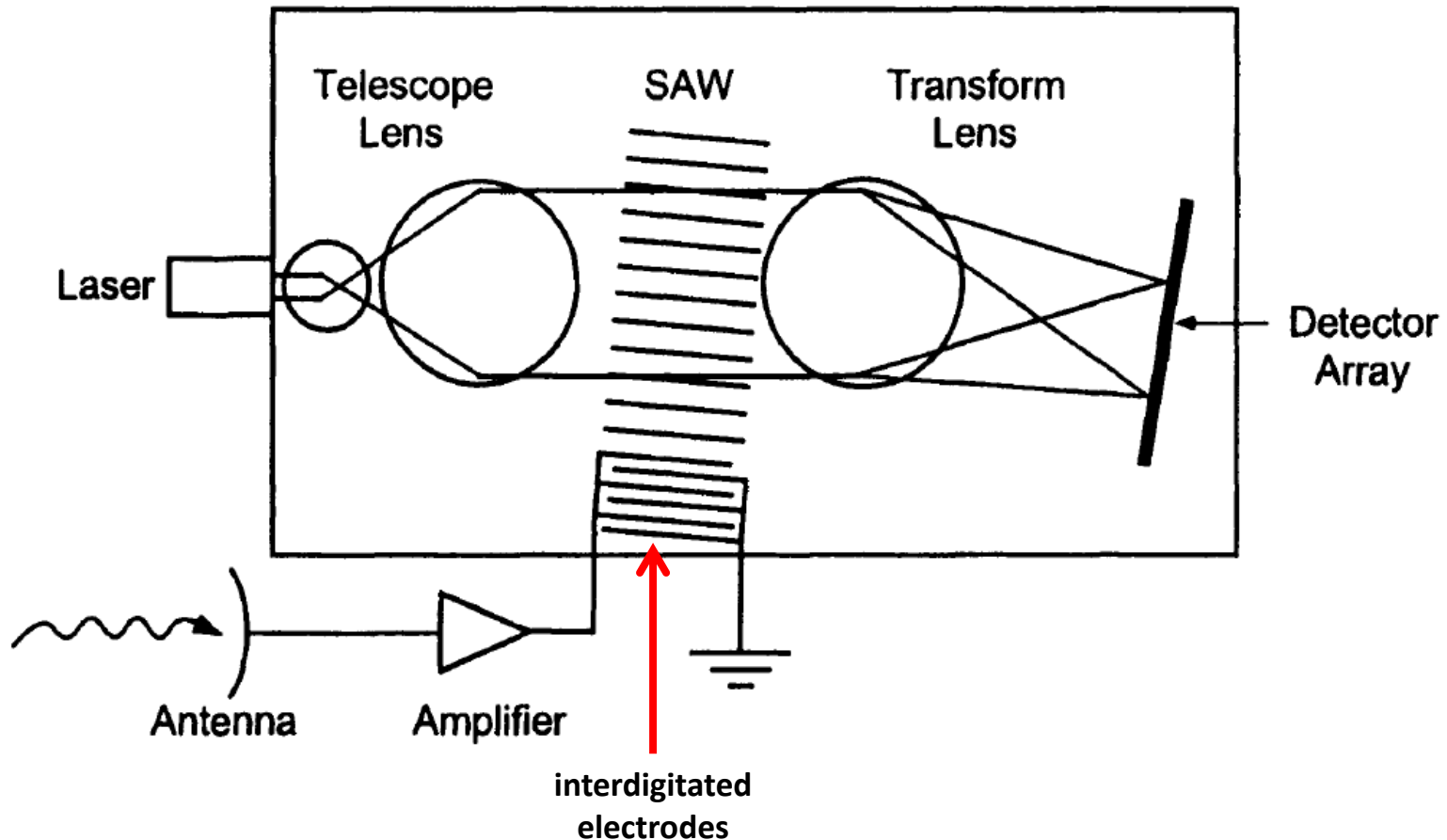


Spectral detection of radio signals

One of the most significant examples of acousto-optic modulation applications in integrated optics is in spectral analysis of radio frequency signals.

A direct application of this device is to allow a pilot to obtain an instantaneous spectrum analysis of a radar signal, in order to determine if the plane is being tracked by a ground-based station, air-to-air missile, or other vehicle. The signature of the radar signal can be deciphered to extract this information.

Spectral detection of radio signals



The Surface Acoustic Wave (SAW) is generated by the incoming electrical signal. An antenna collects the RF signal, and sends it to an amplifier. The amplified signal is applied to an interdigitated array of electrodes on the surface of the planar waveguide.

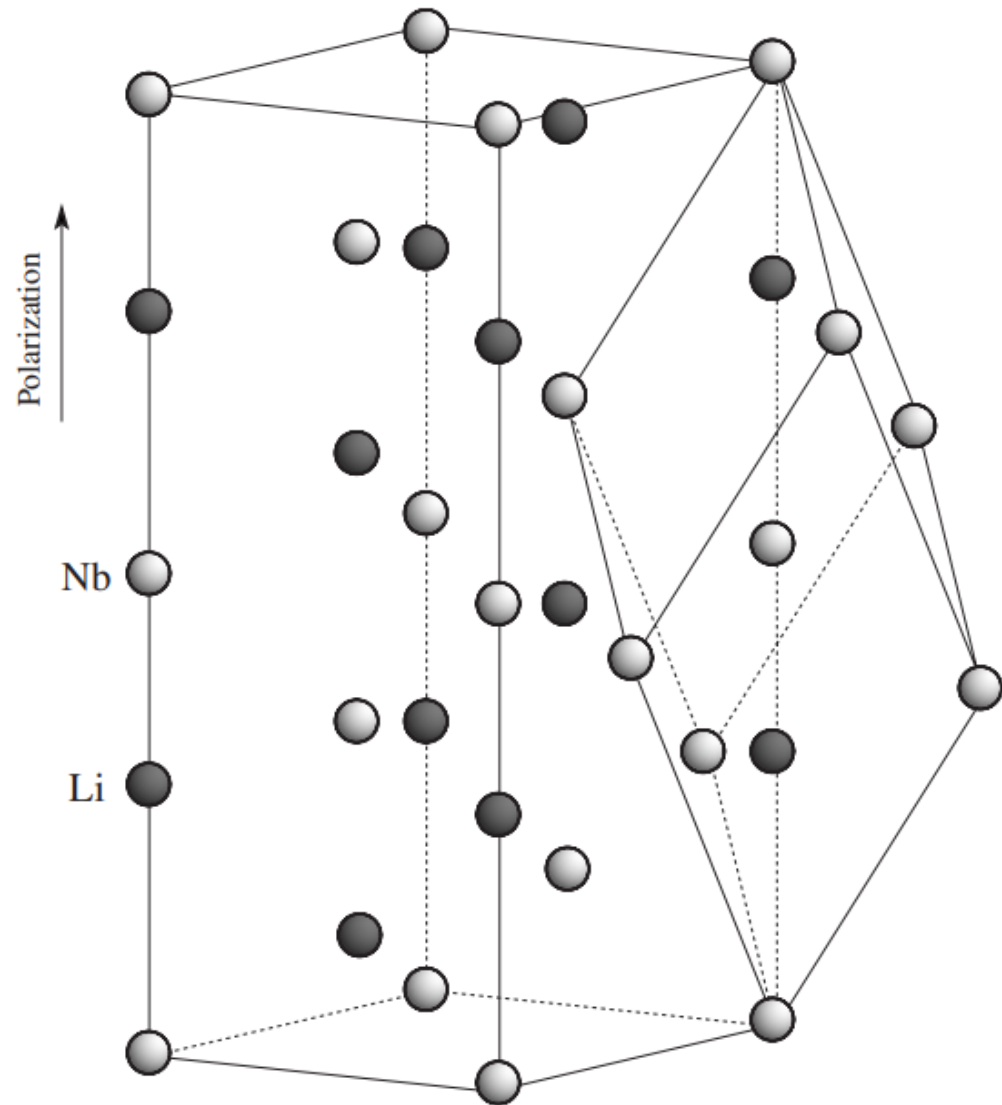
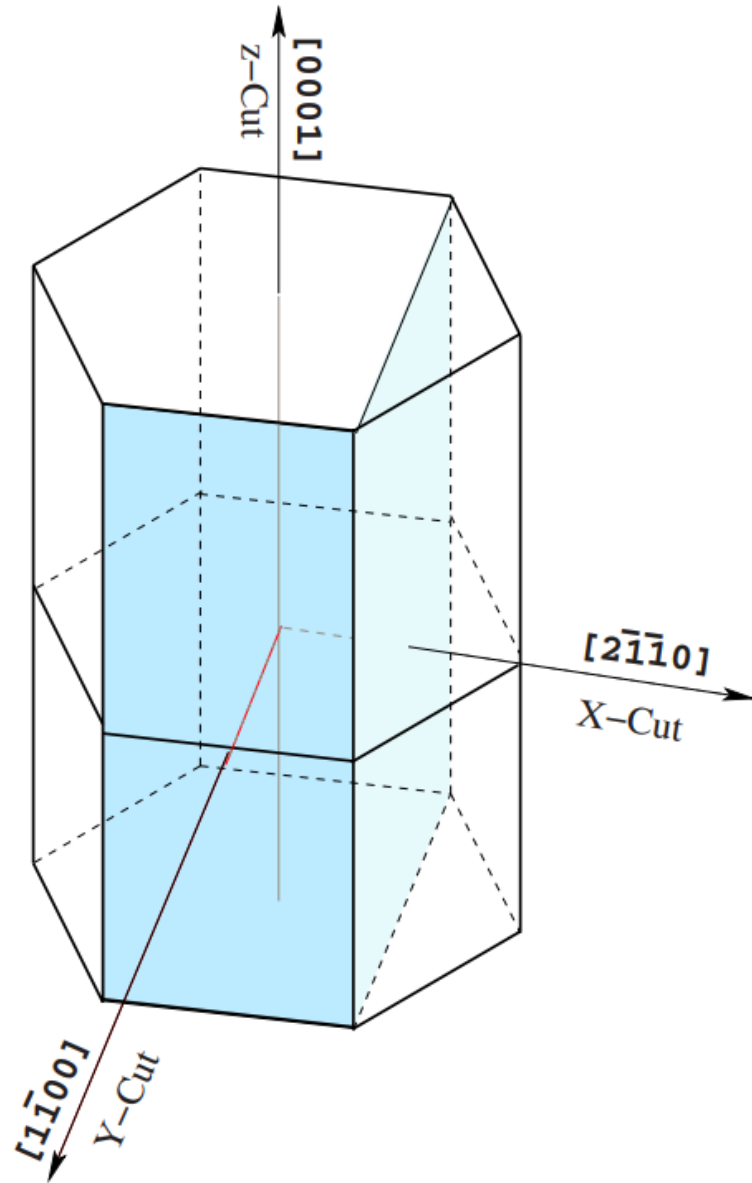
Acousto-optic Modulators

With a piezoelectric material, such as X-cut LiNbO₃, the electric field between the fingers of the electrode periodically constrict and expand the surface material, establishing an acoustic wave that propagates across the waveguide.

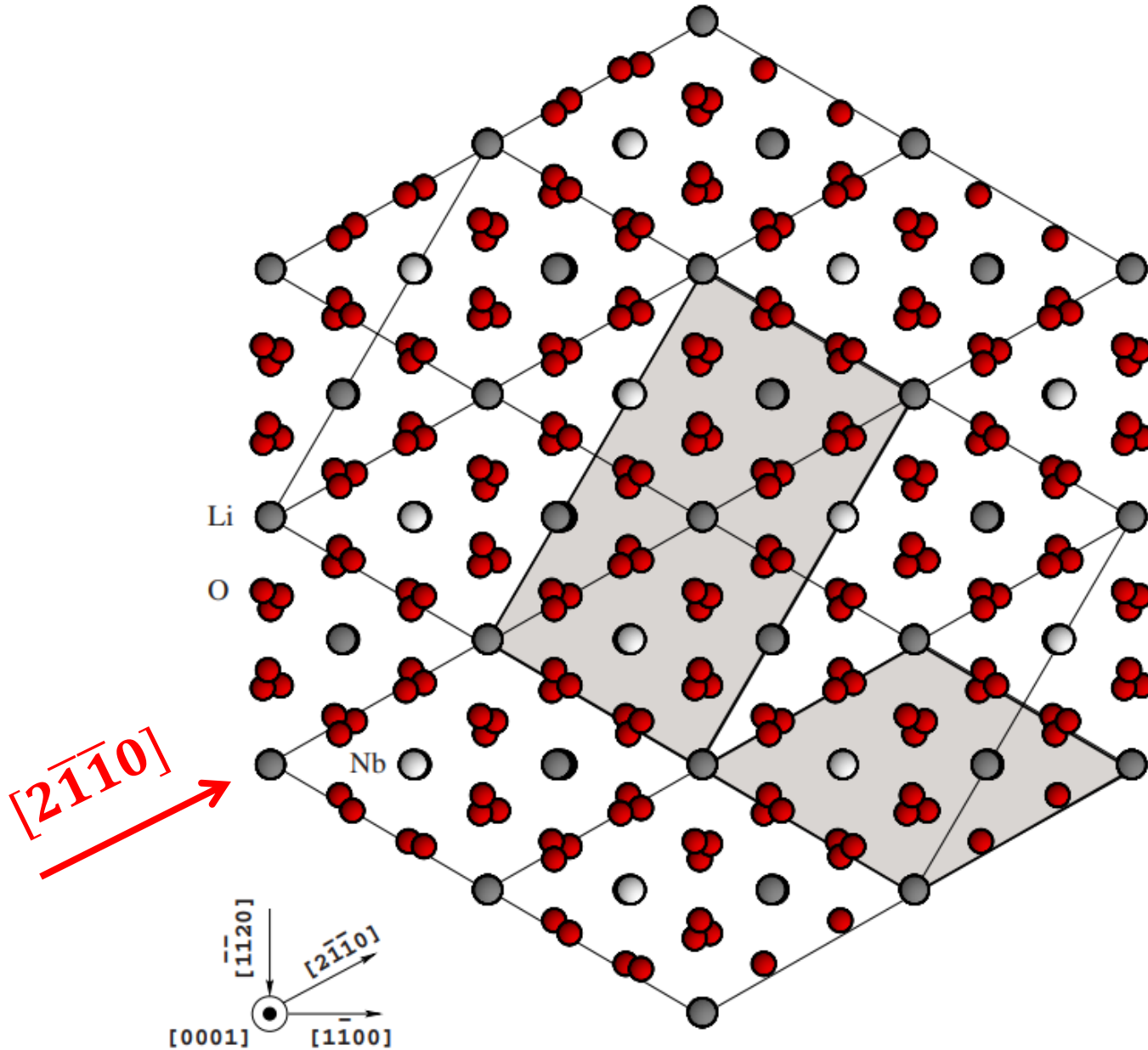
The spatial period of the acoustic wave depends on the frequency of the applied RF signal.

LiNbO₃

(Oxygen omitted)



LiNbO₃ X-cut



Spectral detection of radio signals

The optical beam leaving the SAW region contains several distinct beams travelling in different directions, depending on the spectral content of the applied electrical signal. But the beams are essentially fully spatially overlapped.

To separate the beams, a lens converts the angular variation of the incoming rays (k-space description) into a spatial variation (x-space) at the focus of the output beam (equivalent to a Fourier Transform). The focused output of this lens is directed onto an array of detectors, each one corresponding to a specific frequency of the incoming electrical signal.

All frequencies present in the incoming signal are simultaneously detected at the array, so a *signature* of the signal can be readily determined.

Plasmonic modulation

Plasmonics

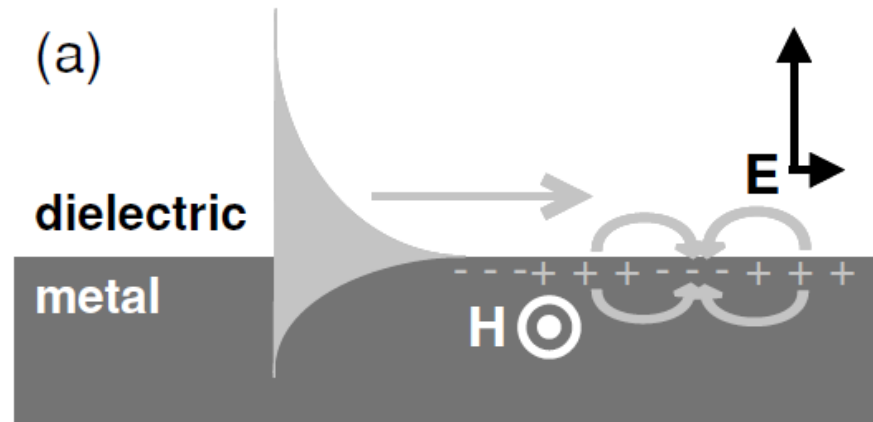
Plasmonics is an extension of **Photonics** and it refers to the generation, detection, and manipulation of optical signals at nanoscale metal-dielectric interfaces.

Plasmonics utilizes **surface plasmon polaritons** (SPPs) which are **coherent electron oscillations** travelling together with an electromagnetic wave at the interface between a dielectric (glass, air, etc.) and a metal (silver, gold, etc.)

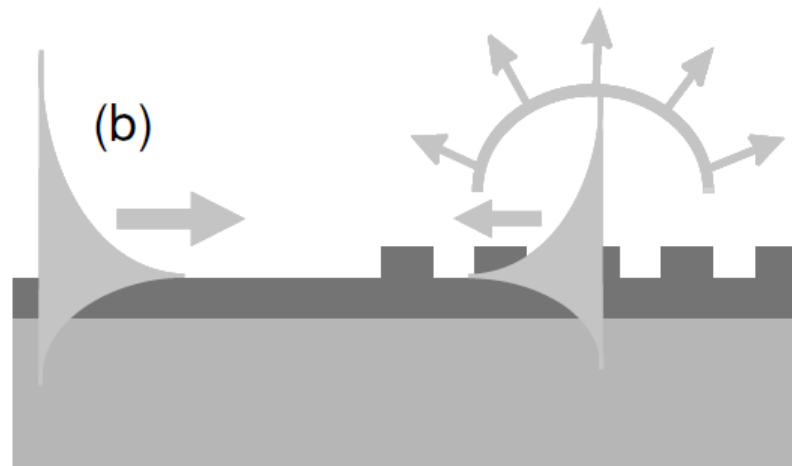
Because of ohmic losses, surface plasmons are limited to travel distances on millimeter scale. Surface roughness is also a limitation. New low-loss plasmonic materials are being investigated, including metal oxides and nitrides.

Plasmonics

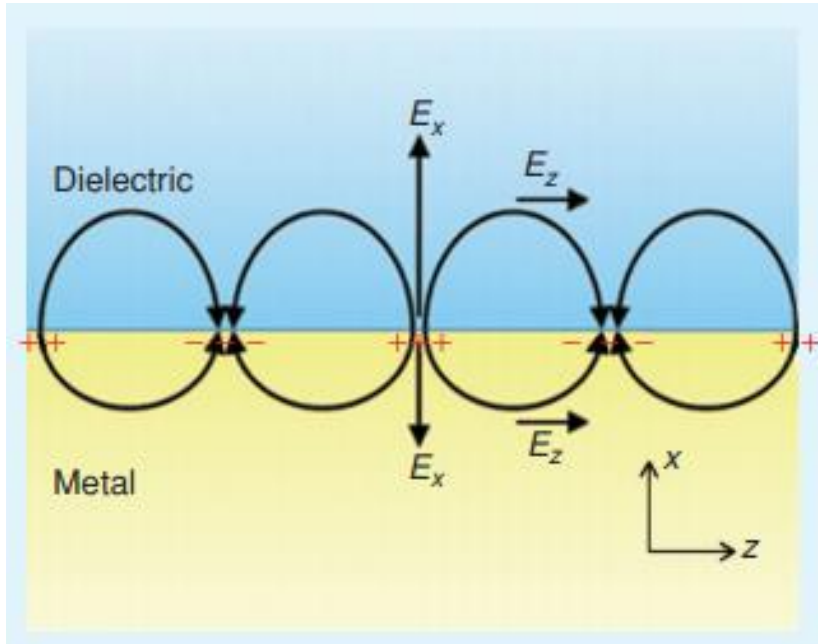
In a plasmonic structure a waveguide can be realized with a single metallic interface



A grating can reflect and scatter the wave. Scattering increases losses.

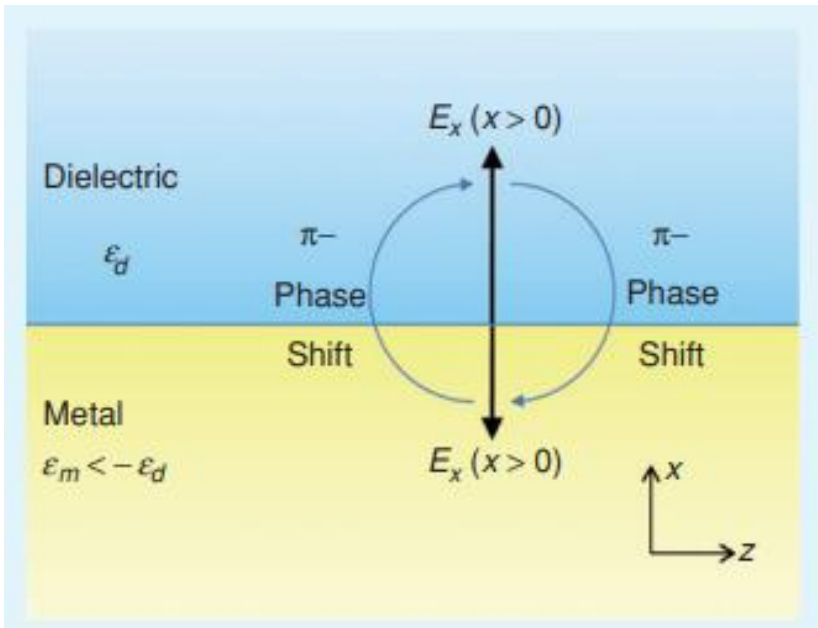


Plasmonics



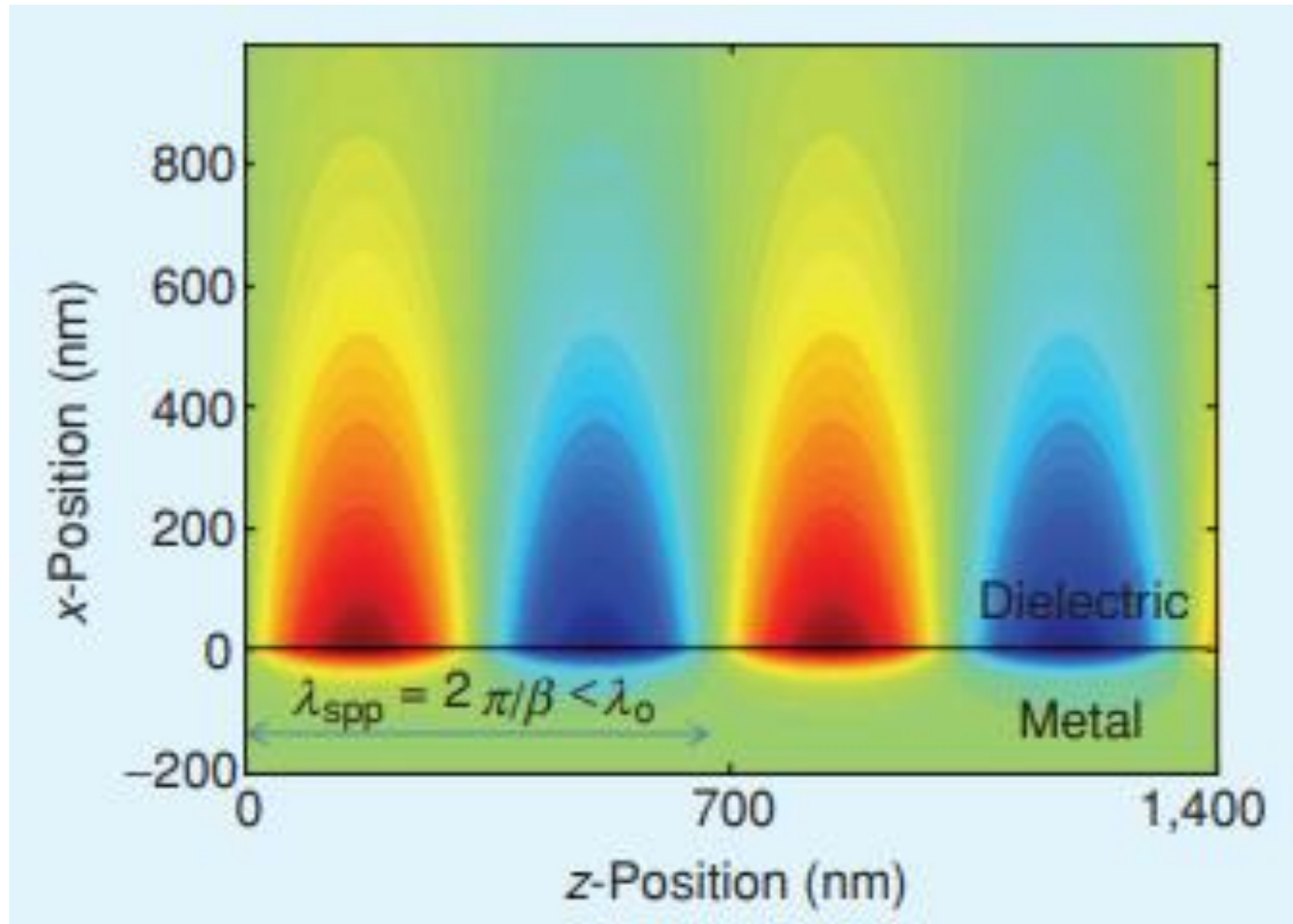
Schematic representation of SPP as charge oscillations at the interface between a metal and a dielectric.

The electric field has a longitudinal (z) component $\pi/2$ out-of-phase with the transverse (x) component.



SPP self-consistency condition allowed by a negative relative permittivity in the metal. The EM wave has phase-shift of π upon crossing the boundary, allowing self-consistency when crossing the boundary twice. This enables the SPP wave guide mode to exist at a single interface.

Plasmonics



Calculated transverse magnetic field (y-direction) for an SPP above gold for $\lambda_0 = 700$ nm.

Single Plasmon Mode for a Single Interface

To form a mode, that decays in both directions away from the surface but is guided along the z -direction, we need TM polarization:

$$\mathbf{H} = H_y \hat{y} = \hat{y} H_0 e^{ik_z z} \begin{cases} e^{-\alpha_1 x} & \text{for } x \geq 0 \\ e^{\alpha_2 x} & \text{for } x \leq 0 \end{cases}$$

The wave equation in each region results in:

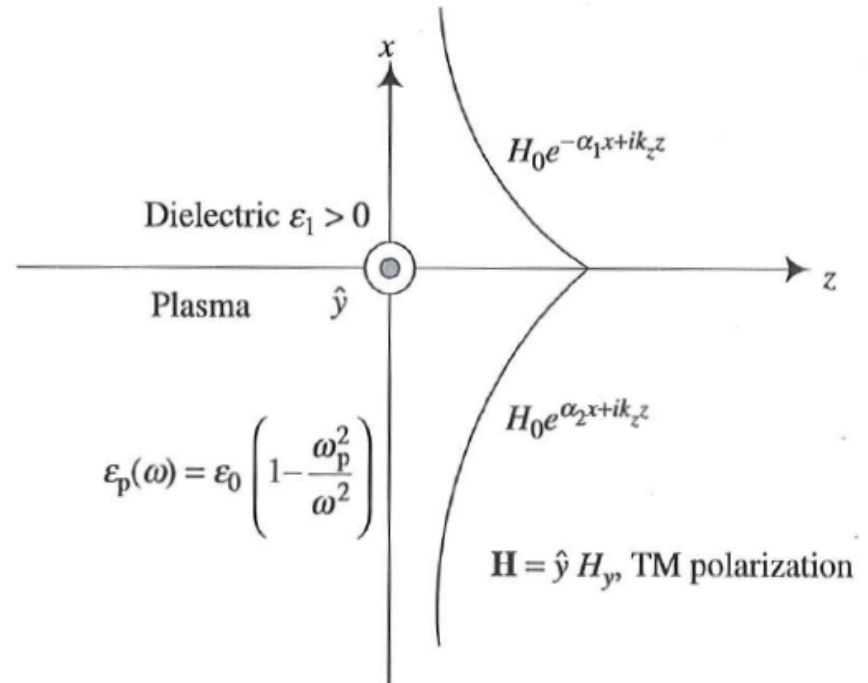
$$-\alpha_1^2 + k_z^2 = \omega^2 \mu_0 \epsilon_1$$

$$-\alpha_2^2 + k_z^2 = \omega^2 \mu_0 \epsilon_p(\omega)$$

The electric field is obtained from

Maxwell's equations $\mathbf{E} = \nabla \times \mathbf{H} / (-i\omega\epsilon)$:

$$\mathbf{E} = \begin{cases} \frac{1}{i\omega\epsilon_1} (\alpha_1 \hat{z} + \hat{x} i k_z) H_0 e^{ik_z z} e^{-\alpha_1 x} & \text{for } x \geq 0 \\ \frac{1}{i\omega\epsilon_p} (-\alpha_2 \hat{z} + \hat{x} i k_z) H_0 e^{ik_z z} e^{\alpha_2 x} & \text{for } x \leq 0 \end{cases}$$



Surface Plasmon Mode for a Single Interface

The tangential component for \mathbf{E} , i.e. E_z must be continuous:

$$\frac{\alpha_1}{\epsilon_1} = -\frac{\alpha_2}{\epsilon_p}$$

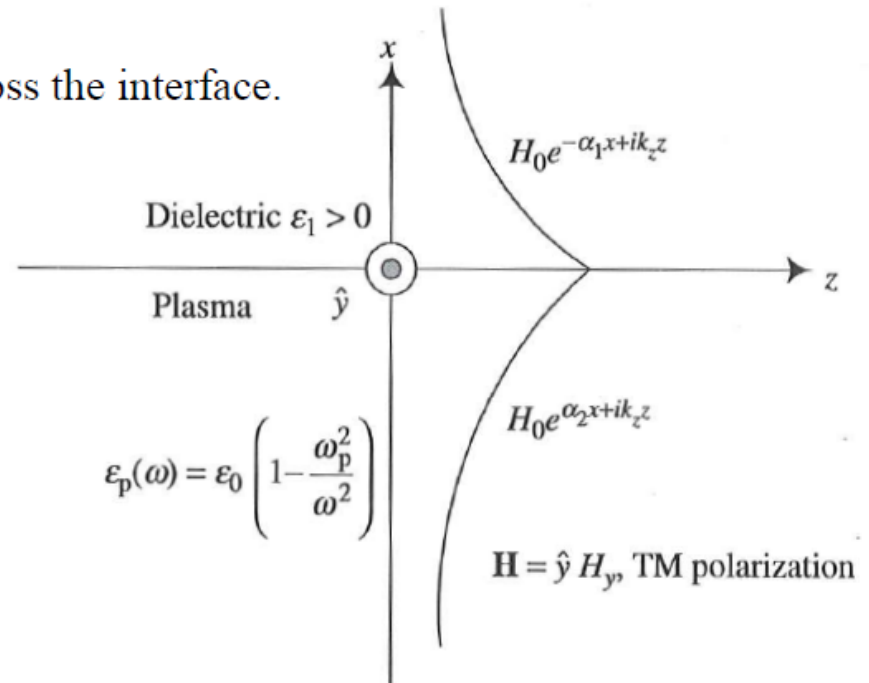
This explains why $\text{Re}[\epsilon]$ needs to change sign across the interface.

Overall, if $\epsilon_p < -\epsilon_1 < 0$, we obtain real solutions:

$$\alpha_1 = \omega \sqrt{\frac{-\mu_0 \epsilon_1^2}{\epsilon_1 + \epsilon_p}}$$

$$\alpha_2 = \omega \sqrt{\frac{-\mu_0 \epsilon_p^2}{\epsilon_1 + \epsilon_p}}$$

$$k_z = \omega \sqrt{\frac{\mu_0 \epsilon_1 \epsilon_p}{\epsilon_1 + \epsilon_p}}$$



The Poynting vector is given by:
$$P = \frac{1}{2} \text{Re}[\mathbf{E} \times \mathbf{H}] = \hat{z} \frac{k_z}{2\omega} |H_0|^2 \begin{cases} \frac{1}{\epsilon_1} e^{-2\alpha_1 x} & \text{for } x \geq 0 \\ \frac{1}{\epsilon_p} e^{2\alpha_2 x} & \text{for } x \leq 0 \end{cases}$$

Surface Plasmon Mode for a Double Interface

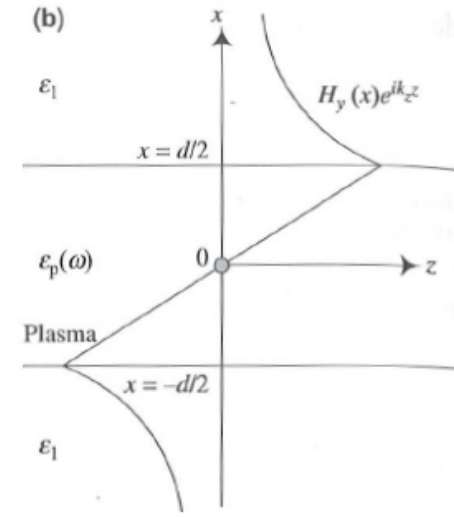
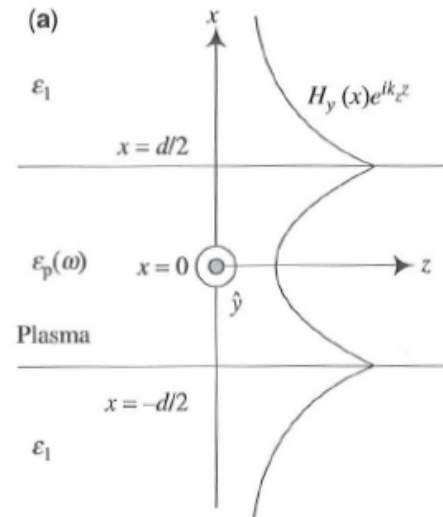
Even and odd TM modes are guided:

$$\mathbf{H}_{\text{even}} = \hat{y} e^{ik_z z} \begin{cases} C_0 e^{-\alpha_1(x-d/2)} & x \geq d/2 \\ C_1 \cosh \alpha_2 x & |x| \leq d/2 \\ C_0 e^{\alpha_1(x+d/2)} & x \leq -d/2 \end{cases}$$

The wave equation in each region results in:

$$-\alpha_1^2 + k_z^2 = \omega^2 \mu_0 \epsilon_1$$

$$-\alpha_2^2 + k_z^2 = \omega^2 \mu_0 \epsilon_p(\omega)$$



We need H_y and E_z to be continuous at $x = \pm \frac{d}{2}$ [Use: $\mathbf{E} = \nabla \times \mathbf{H} / (-i\omega\epsilon)$]

$$C_0 = C_1 \cosh \alpha_2 \frac{d}{2} \quad \text{and} \quad -\frac{\alpha_1}{\epsilon_1} C_0 = C_1 \frac{\alpha_2}{\epsilon_p} \sinh \alpha_2 \frac{d}{2}. \quad \text{Dividing these two gives:}$$

$$\alpha_1 = -\frac{\epsilon_1}{\epsilon_p} \alpha_2 \tanh \alpha_2 \frac{d}{2} \quad (\text{boundary condition})$$

$$\alpha_2^2 - \alpha_1^2 = \omega^2 \mu_0 (\epsilon_1 - \epsilon_p) \quad (\text{wave equation})$$

Surface Plasmon Mode for a Double Interface

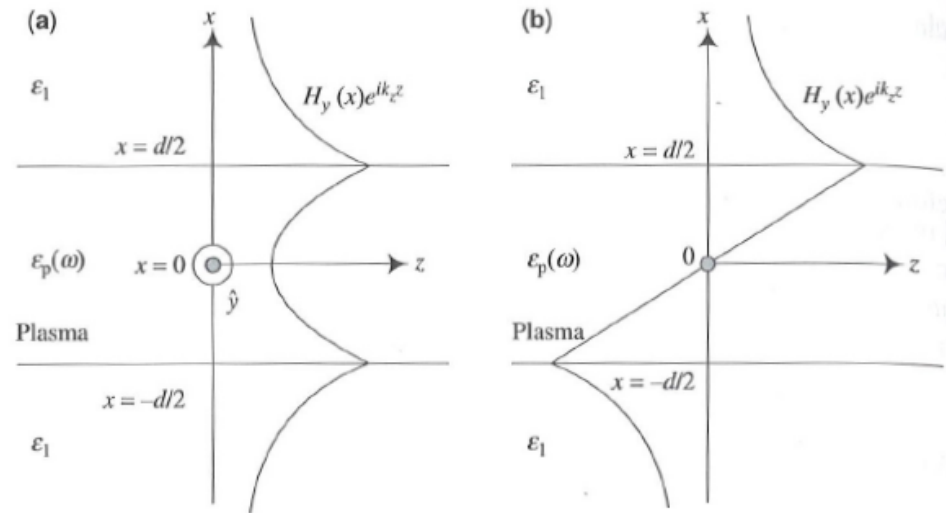
Even and odd TM modes are guided:

$$\mathbf{H}_{odd} = \hat{y} e^{ik_z z} C_1 \begin{cases} \sinh \alpha_2 \frac{d}{2} e^{-\alpha_1 (x - \frac{d}{2})} & x \geq d/2 \\ \sinh \alpha_2 x & |x| \leq d/2 \\ -\sinh \alpha_2 \frac{d}{2} e^{\alpha_1 (x + \frac{d}{2})} & x \leq -d/2 \end{cases}$$

The same analysis yields:

$$\alpha_1 = -\frac{\epsilon_1}{\epsilon_p} \alpha_2 \coth \alpha_2 \frac{d}{2} \quad (\text{boundary condition})$$

$$\alpha_2^2 - \alpha_1^2 = \omega^2 \mu_0 (\epsilon_1 - \epsilon_p) \quad (\text{wave equation})$$



Surface Plasmon Mode for a Double Interface

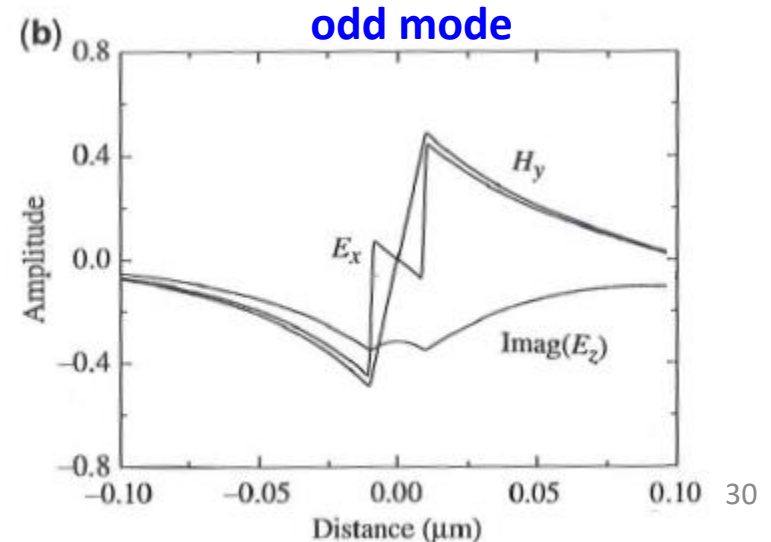
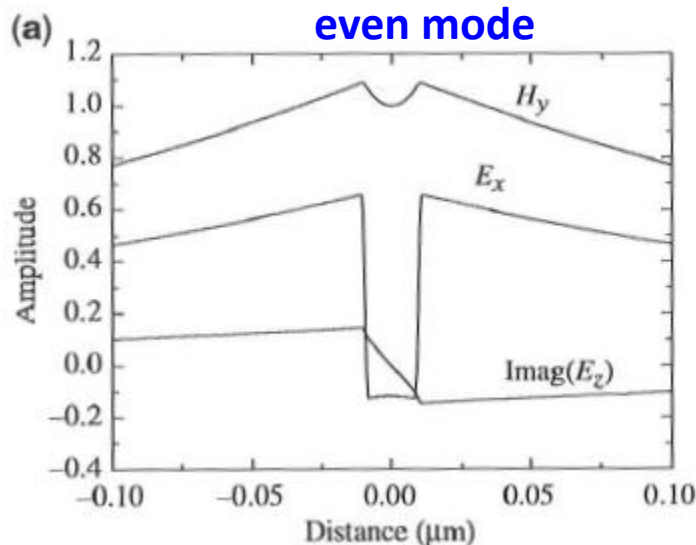
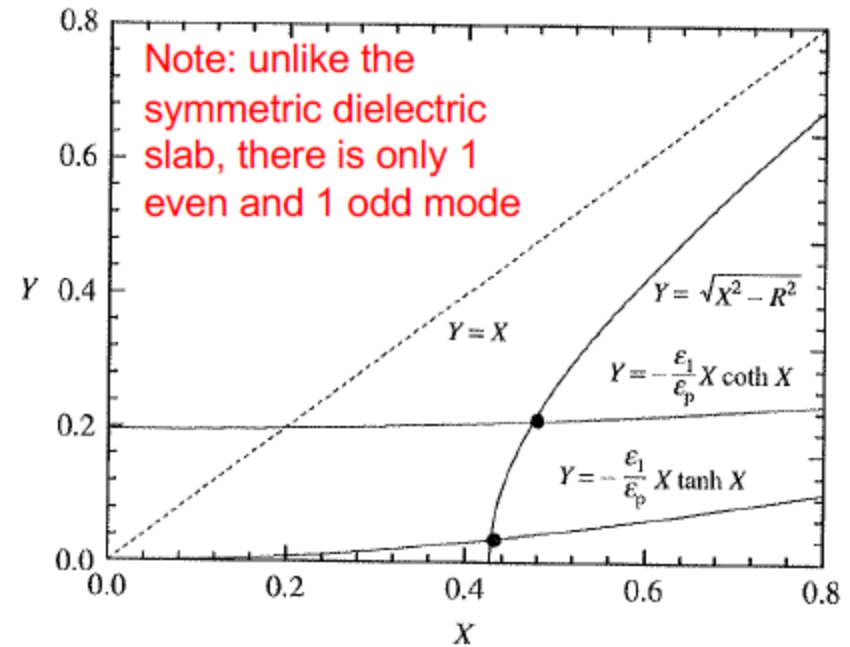
For both even and odd modes, we define:

$$X = \alpha_2 \frac{d}{2}, Y = \alpha_1 \frac{d}{2}, R = \omega \sqrt{\mu_0 (\epsilon_1 - \epsilon_p)} \frac{d}{2},$$

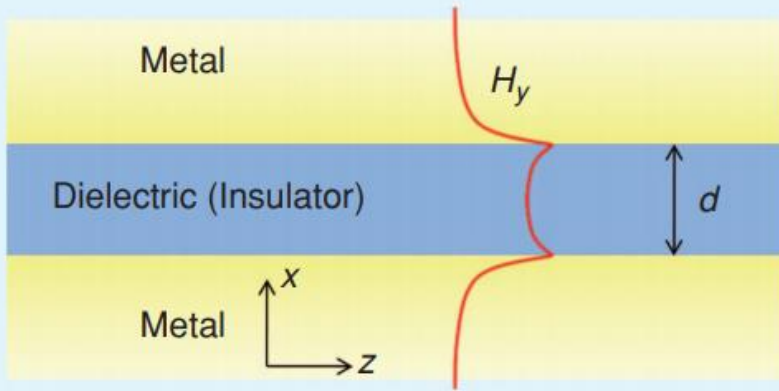
We need to solve:

$$X^2 - Y^2 = R^2 \quad (\text{wave equation})$$

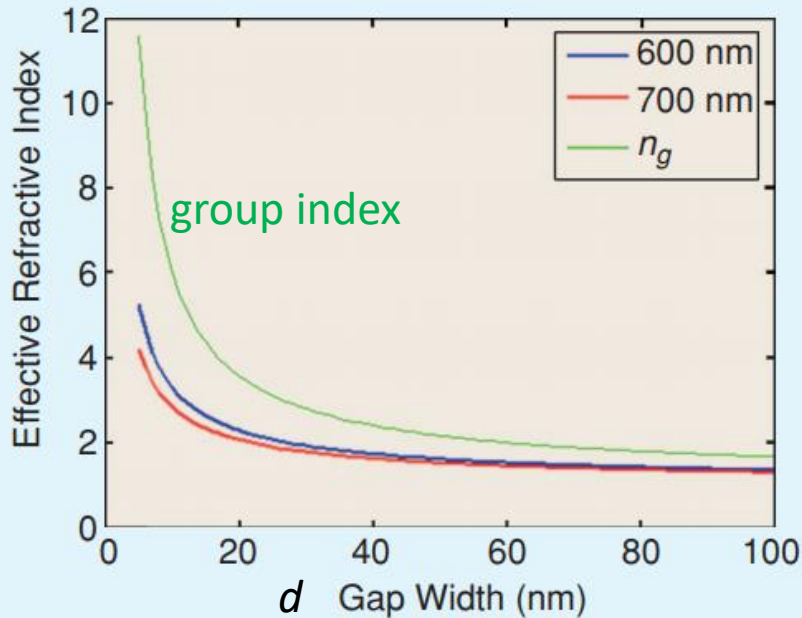
$$Y = \begin{cases} -\frac{\epsilon_1}{\epsilon_p} X \tanh X & (\text{even modes}) \\ -\frac{\epsilon_1}{\epsilon_p} X \coth X & (\text{odd modes}) \end{cases}$$



MIM structure



(a)



(b)

Calculate effective index from this relation

$$\tanh \left(\frac{d}{2} \sqrt{\beta^2 - \left(\frac{\omega}{c}\right)^2 \epsilon_d} \right) =$$

$$- \frac{\epsilon_d}{\epsilon_m} \sqrt{\frac{\beta^2 - \left(\frac{\omega}{c}\right)^2 \epsilon_m}{\beta^2 - \left(\frac{\omega}{c}\right)^2 \epsilon_d}}$$

$$\beta \equiv k_z$$

Light slows down as d is made smaller

Plasmonics

A simple modulator may consist of a single metal stripe embedded in dielectric, with the same stripe being used to guide and control the optical radiation propagating in the form of surface plasmon polaritons (SPPs).

Various hybrid modulator structures have been proposed for integration

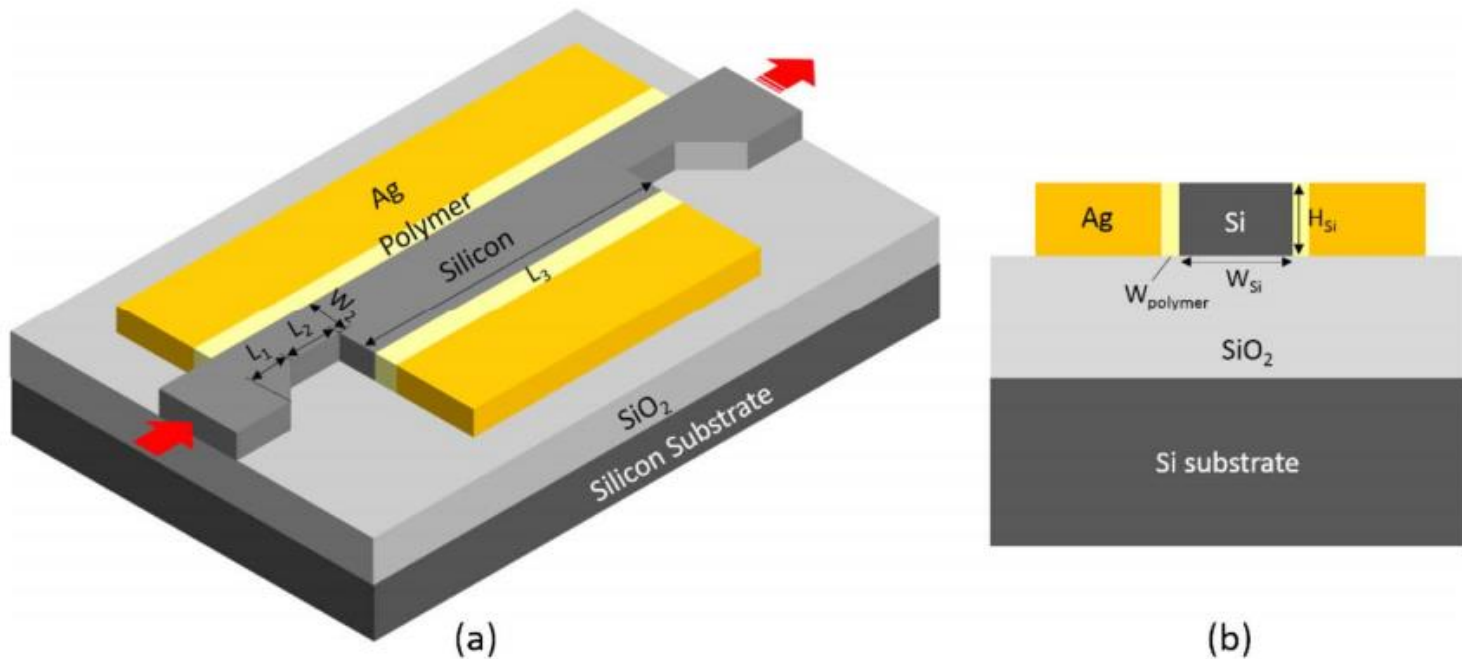


Fig. 1. (a) Schematic perspective view of the proposed optical intensity modulator. L_1 , L_2 , and L_3 are taper, SSHW, and DSHW lengths, respectively. (b) Cross-sectional view of the DSHW.

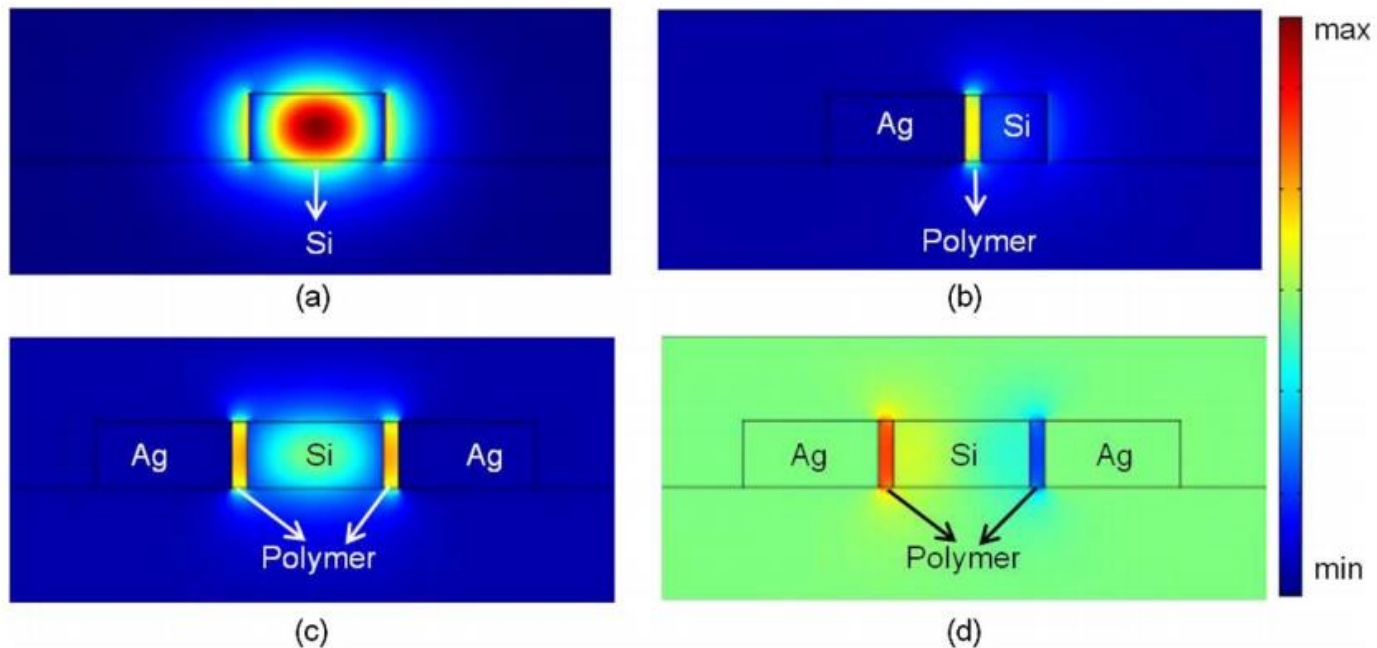
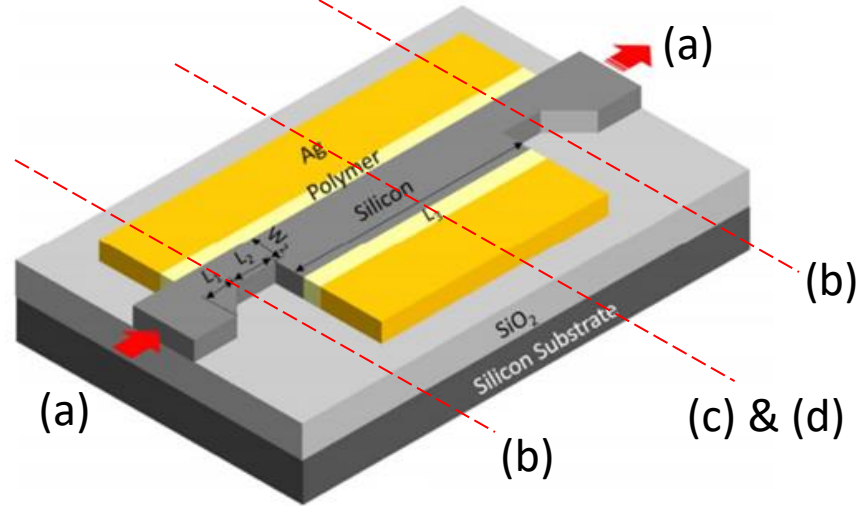


Fig. 2. Transverse electric field mode patterns for various waveguide modes: (a) Input/output silicon waveguide mode, (b) SSHW mode, (c) DSHW quasi-even mode, and (d) DSHW quasi-odd mode. $W_{Si} = 450$ nm, $H_{Si} = 250$ nm, and $W_{polymer} = 50$ nm.

Plasmonics

Metal based plasmonics have limitation, such as fixed plasma frequency in the material (limited range of operation frequencies) and integration challenges. Recent investigations look at semiconductor-based plasmonic devices.

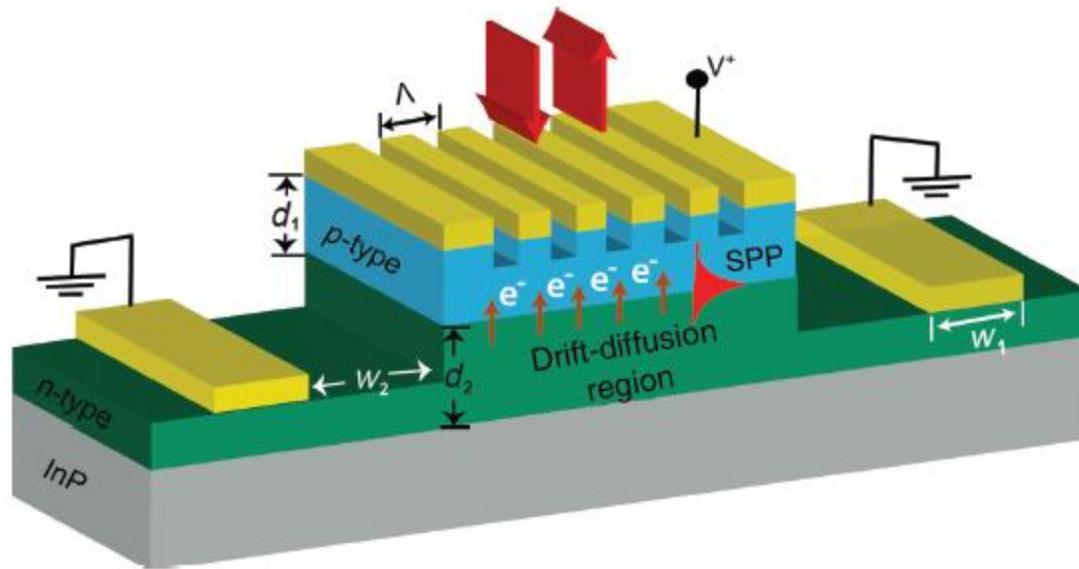


Figure 1: Basic schematic of the surface plasmon polariton diode (SPPD).

The SPPD consists of a lattice-matched indium gallium arsenide ($\text{In}_{0.53}\text{Ga}_{0.47}\text{As}$) pn^{++} junction grown epitaxially on an indium phosphide (InP) substrate. A grating with period $\Lambda = 2.4 \mu\text{m}$ is used to couple mid-IR incident light to the surface plasmon polariton (SPP) modes propagating the junction interface. The relevant device sizes are as follows; $d_1 = 0.75 \mu\text{m}$, $d_2 = 1 \mu\text{m}$, $w_1 = 100 \mu\text{m}$, and $w_2 = 50 \mu\text{m}$.

Vinnakota et al., Nanophotonics 2020; 9(5): 1105–1113

Reading Assignments:

- Section 12.1 of Chuang's book
- Chapter 8 of Chuang's book
- Chapter 13 of Chuang's book

Photodetectors

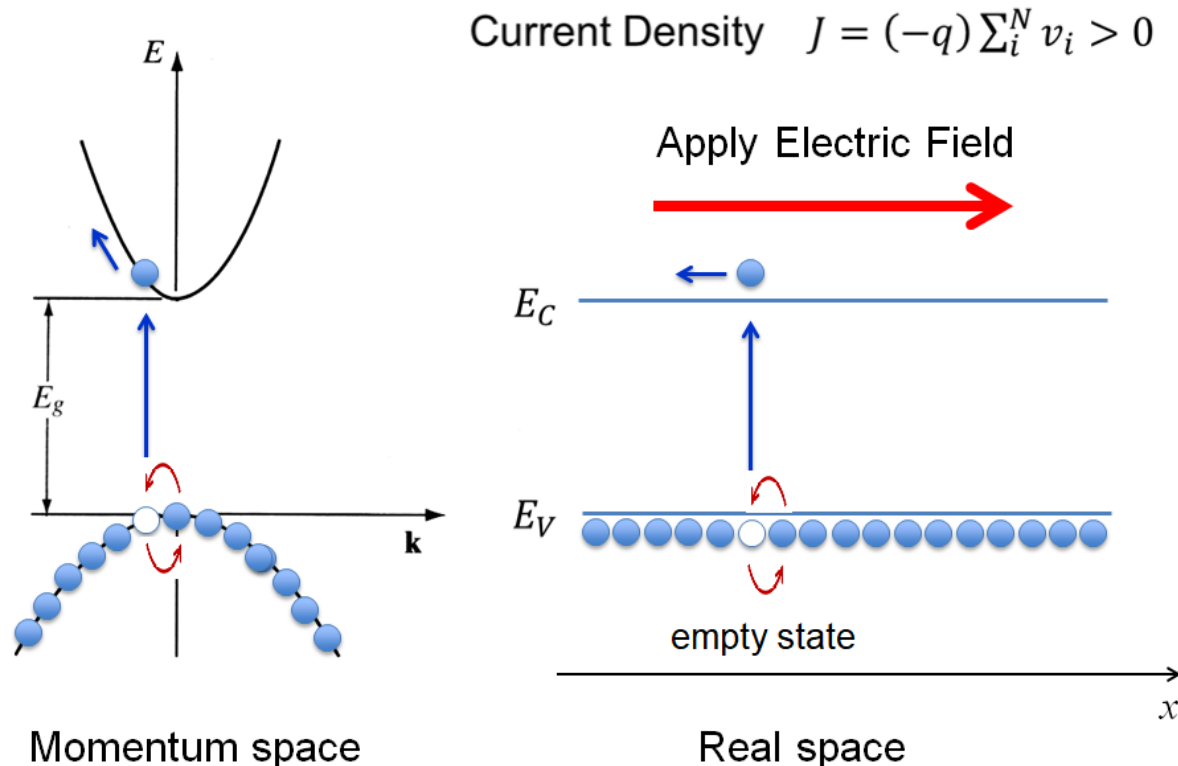
A photodetector converts light into an electric current for a variety of application:

- **Receivers in optical communications**
- **Laser monitoring**
- **Optical position sensing for automatic control of machinery**
- **Opto-isolators for interference-free coupling between electrical circuits**
- **Digital Photography**
- **Non-photographic recording of astronomical images**
- **Thermography**
- **etc...**

Photodetectors

In general, the most efficient means of photodetection in solid-state devices occurs by interband photon absorption with the energy used to create an electron-hole pair.

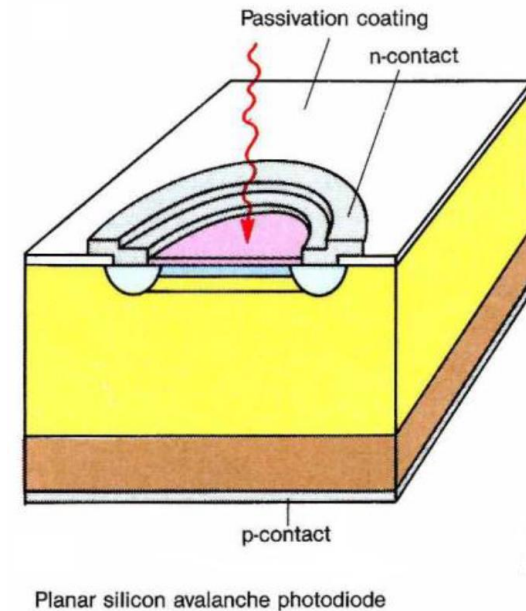
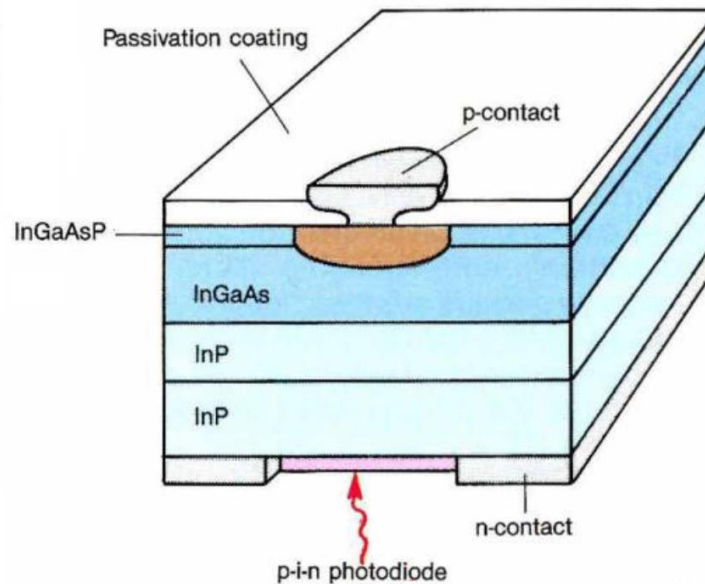
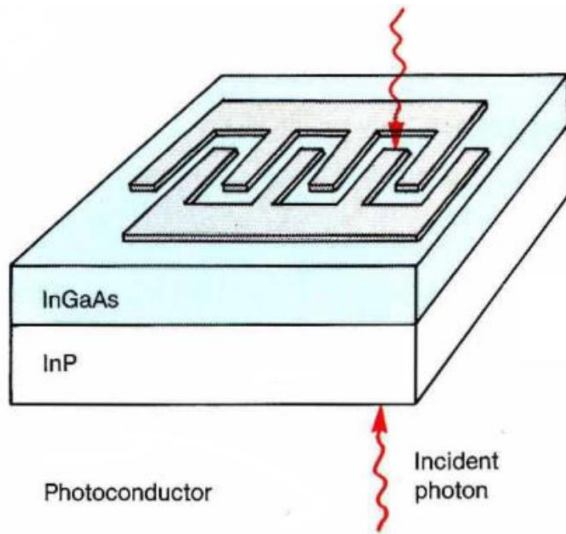
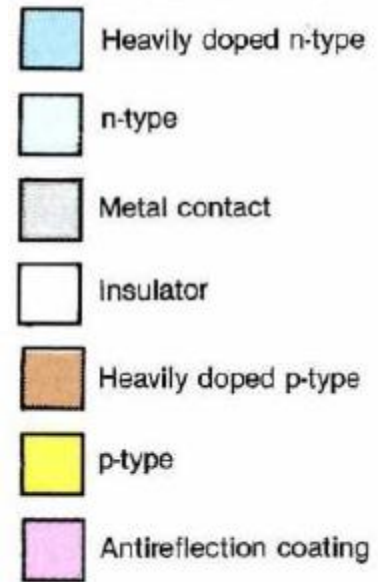
The two types of carriers are separated by an electric field before they recombine and the two flows in different directions generates a photocurrent.



Photodetectors

There are three broad categories of photodetectors:

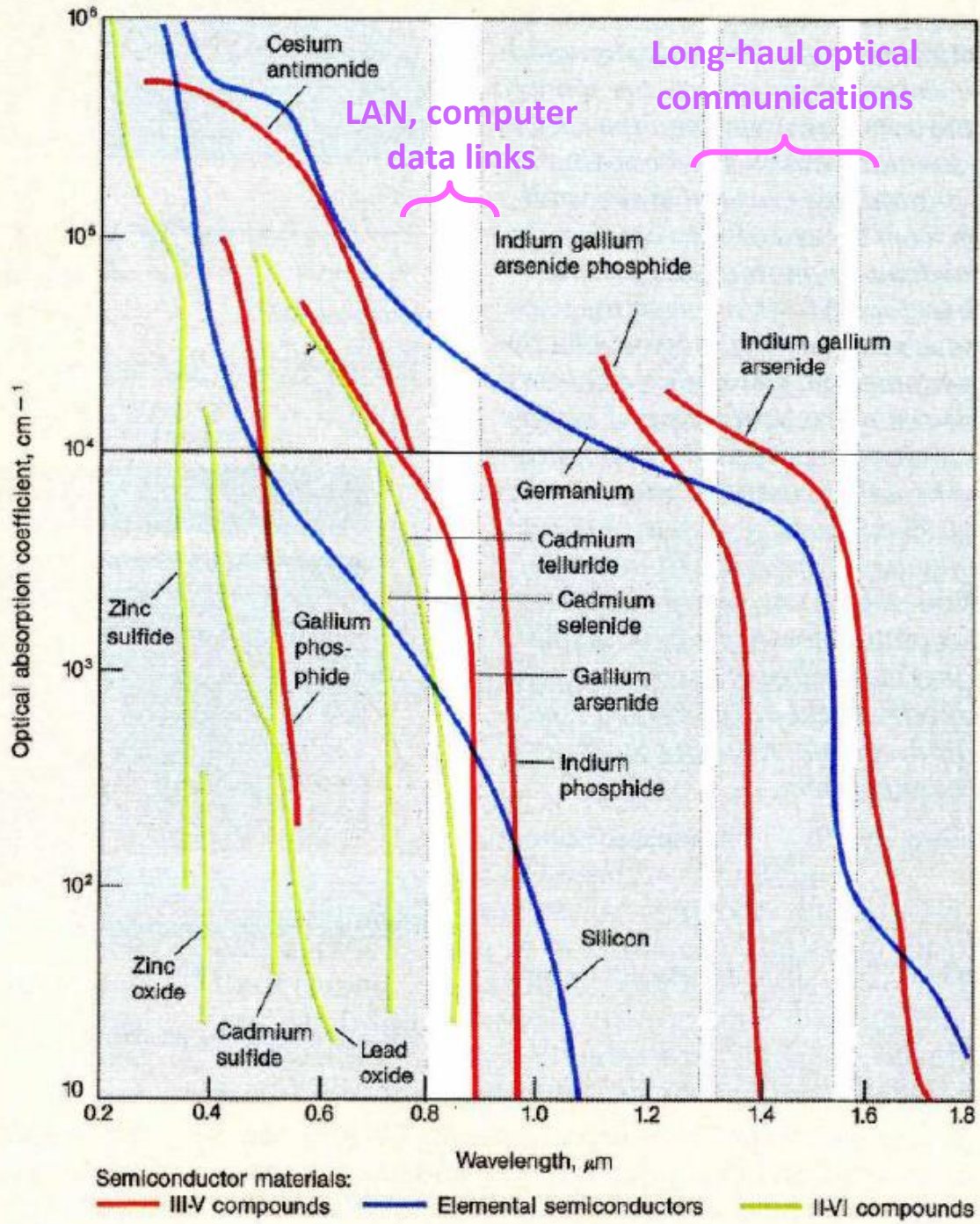
- Photoconductors
- Junction-based photodiodes (e.g., *p-i-n* diode)
- Avalanche photodiodes



Photodetectors

Important properties to consider in photodetectors are:

- **Sensitivity**
- **Gain**
- **Noise**
- **Bandwidth**
- **Response to specific frequencies of interest**



Absorption coefficients of materials used in various optical applications

Most desirable range for high performance applications

IEEE SPECTRUM MAY 1986

Typical photodiode materials are:

- silicon (Si): low **dark current**, high speed, good sensitivity between roughly 400 and 1000 nm (best around 800–900 nm)
- germanium (Ge): high dark current, slow speed due to large parasitic capacity, good sensitivity between roughly 900 and 1600 nm (best around 1400–1500 nm)
- indium gallium arsenide phosphide (InGaAsP): expensive, low dark current, high speed, good sensitivity roughly between 1000 and 1350 nm (best around 1100–1300 nm)
- indium gallium arsenide (InGaAs): expensive, low dark current, high speed, good sensitivity roughly between 900 and 1700 nm (best around 1300–1600 nm)

Photoconductors

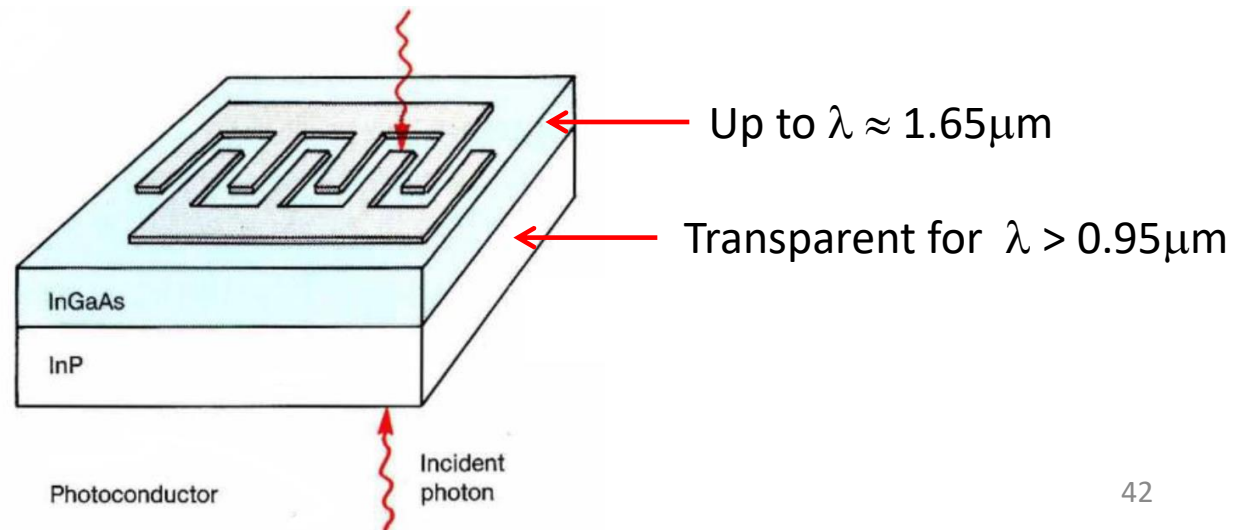
In a photoconductor material, electrical conductivity increases with illumination.

For long-wavelength applications a thin layer of $\text{In}_{0.53}\text{Ga}_{0.47}\text{As}$ is typically used. The top metallic layer has interdigitated anode and cathode to maximize the light reaching the conducting layer and minimize the distance that photogenerated carriers must travel before being collected at one of the electrodes (to improve bandwidth).

The conducting layer may be 1 to $2\mu\text{m}$ deep, thick enough to absorb a significant fraction of incident light but also thin enough to minimize the noise current resulting from the low resistivity of the semiconductor layer.

Quantum efficiency (# of e-h pairs generated per incident photon) depends on the thickness and on the absorption coefficient of the layer. A $2\mu\text{m}$ layer typically gives about 88% quantum efficiency. Antireflecting coating can increase efficiency further.

A current always flows. The signal-to-noise ratio depends on the ratio between conductivity under illumination and conductivity in the dark.



Photoconductors

Continuity equations

$$\frac{\partial n}{\partial t} = G_n - R_n + \frac{1}{q} \frac{\partial}{\partial x} J_n(x)$$

$$\frac{\partial p}{\partial t} = G_p - R_p - \frac{1}{q} \frac{\partial}{\partial x} J_p(x)$$

At thermal equilibrium

$$G_n = R_n$$

$$G_p = R_p$$

Assume p-type material with $p_0 = N_A$ $n_0 \approx \frac{n_i^2}{N_A}$

Optical generation

$$p = p_0 + \delta p$$

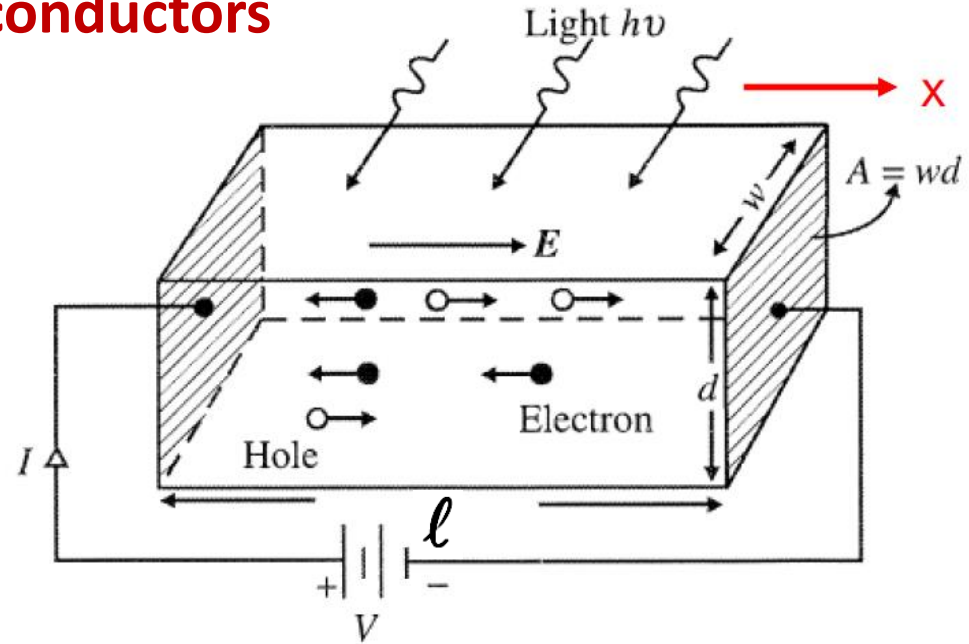
$$n = n_0 + \delta n$$

$$\delta p = \delta n$$

Recombination rate

$$R_n = \frac{\delta n}{\tau_n}$$

Uniform & Constant Generation $G_n(x, t) = G_0 \Rightarrow \delta n = G_0 \tau_n$



Photoconductors

With applied Electric Field, conduction current

$$J = J_n + J_p = q(\mu_n n + \mu_p p) E$$

$$= \sigma E = \sigma \frac{V}{\ell}$$

Without illumination, *dark conductivity*

$$\sigma = q(\mu_n n_0 + \mu_p p_0)$$

With illumination, photoconductivity and photocurrent

$$\Delta\sigma = q(\mu_n \delta n + \mu_p \delta p) = q(\mu_n + \mu_p) G_0 \tau_n$$

$$\Delta I = \Delta\sigma \frac{A}{\ell} V = q(\mu_n + \mu_p) G_0 \tau_n \frac{A}{\ell} V$$

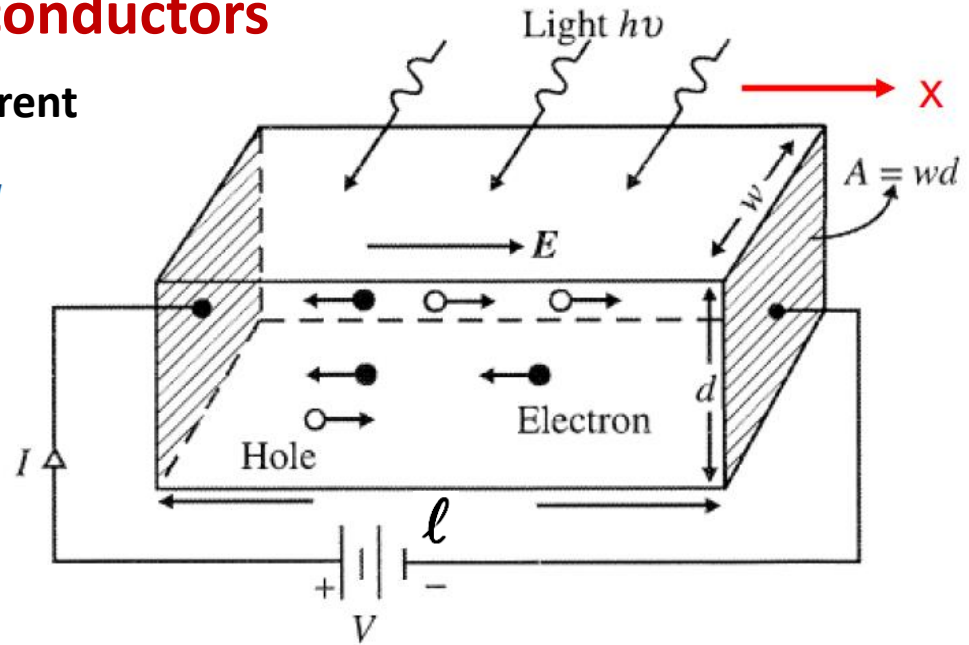
With

$$\mu_n \gg \mu_p$$

$$\mu_n \frac{V}{\ell} = \mu_n E = v_d = \frac{\ell}{\tau_t}$$

drift velocity

transit time



$$\Delta I = q G_0 A \ell \frac{\tau_n}{\tau_t}$$

Photoconductors

$$\Delta I = qG_0 A \ell \frac{\tau_n}{\tau_t}$$

Electron-hole pairs generated in Volume

Photoconductive gain

$$G_0 A \ell \frac{\tau_n}{\tau_t}$$

If we include both electron and hole contributions

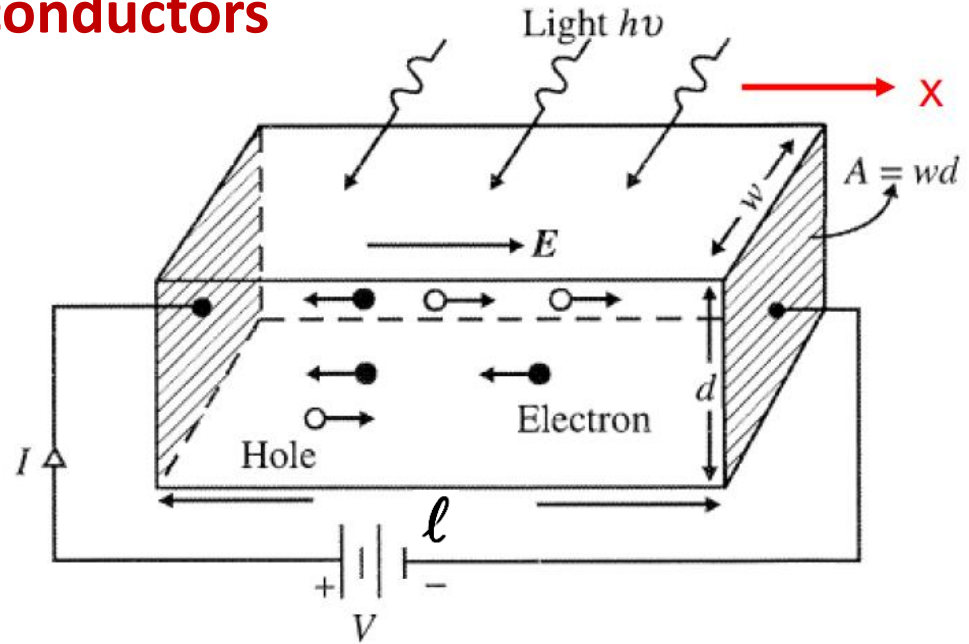
$$\frac{1}{\tau_t} = \frac{1}{\tau_{tn}} + \frac{1}{\tau_{tp}} = \left(\mu_n + \mu_p \right) \frac{E}{\ell}$$

$$\tau_n \ll \tau_t$$

Photocurrent is small

$$\tau_n \gg \tau_t$$

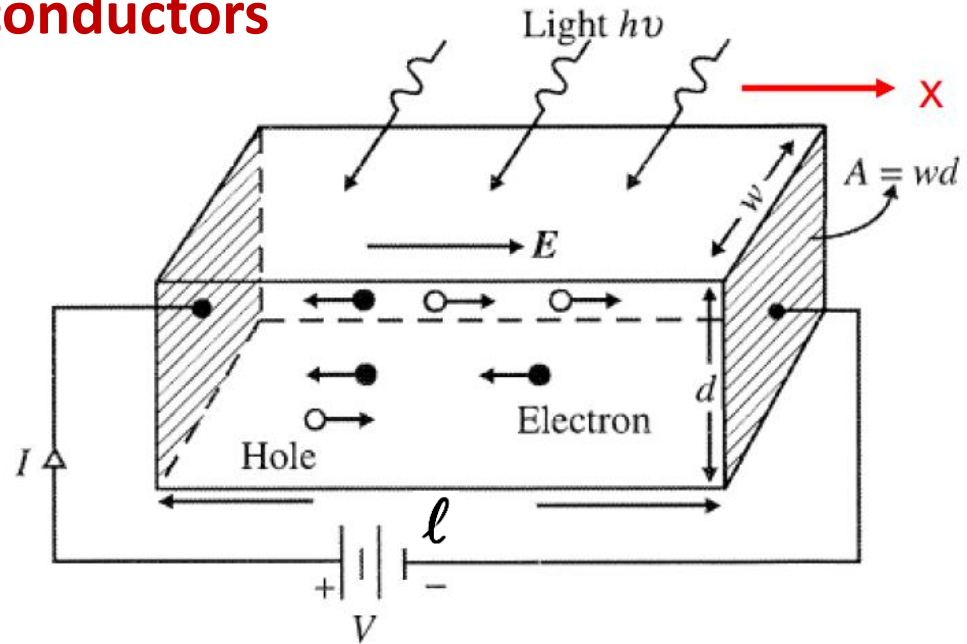
There is photoconductive gain. Many electrons traverse the device before one recombination occurs (as many passes as τ_n/τ_t).



Photoconductors

Since slower positive holes linger in the device, they facilitate injection of negative electrons from the contact, facilitating gain.

However, the higher the gain, the lower the bandwidth.



The most convenient way of expressing this physical tradeoff is the gain-bandwidth product. For given material and device structure, photoconductor gain can only be achieved at the expense of bandwidth.

Gains of 1000 or more can be observed in Si photoconductors. In InGaAs we have only about 50 to 100 gain but with response time of 1 to 2 nanoseconds, suitable for moderate bit-rate applications up to 500 Mbit/s to 1Gbit/s.

Photoconductors

Noise is in general a problem for photoconductors. The lack of a p-n junctions means that current is always present.

Johnson thermal noise is particularly important

$$\text{Thermal Noise: } \langle i_S^2 \rangle = \frac{4k_B T}{R_{eq}} B$$

The signal-to-noise ratio increases with increasing the resistance of the conducting layer. Unfortunately this corresponds to a decrease of frequency response.

The strong points of photoconductors are simplicity and ease of integration, so they are appealing for applications which do not need ultimate performance.

incident power

$$G_0 = \eta \frac{P_{opt} / h\nu}{\ell wd} = \eta \frac{P_{opt} / \hbar\omega}{\ell wd}$$

generation rate

quantum efficiency

Quantum Efficiency η = fraction of photons created by electron-hole pairs

$$\eta = \eta_i (1 - R) (1 - e^{-\alpha d})$$

air-semiconductor Reflectance

absorption coefficient of the optical intensity

injected primary photocurrent

$$I_{ph} = \eta q \frac{P_{opt}}{\hbar\omega}$$

we obtained earlier

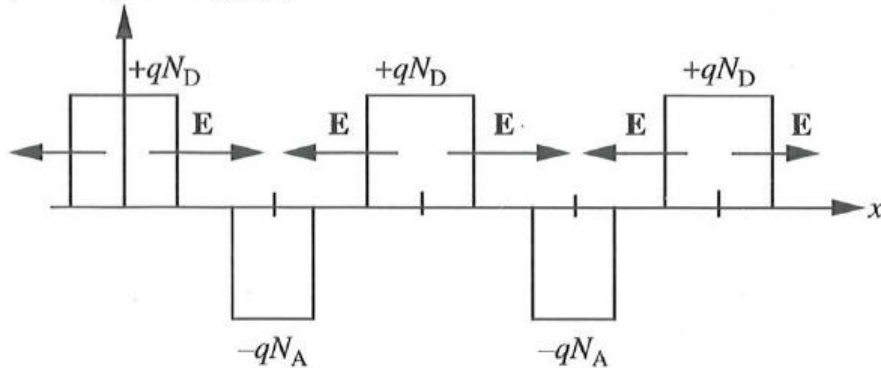
$$\Delta I = q G_0 A \ell \frac{\tau_n}{\tau_t} \Rightarrow \Delta I = \frac{\tau_n}{\tau_t} I_{ph}$$

Photocurrent per unit incident power (Responsivity)

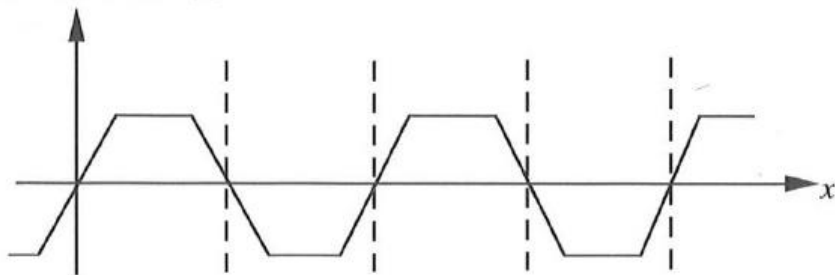
$$R_\lambda (A/W) = \frac{\Delta I}{P_{opt}} = \eta \frac{q}{\hbar\omega} \frac{\tau_n}{\tau_t}$$

n-i-p-i Superlattice Photoconductors

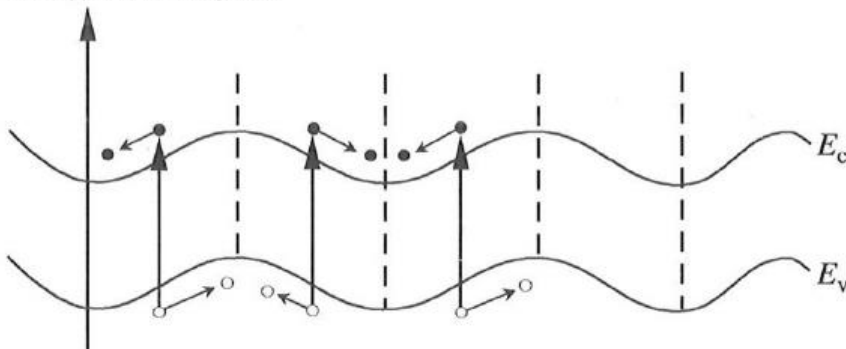
(a) Charge density $\rho(x)$



(b) Electric field $E(x)$



(c) Energy band diagram



Large photoconductive gain may be achieved if carriers are prevented from recombining in the semiconductor.

By using modulation doping, separate channels are created for electrons and holes, where they drift or diffuse into after being created.

The recombination lifetime can be made many of order of magnitude larger than in bulk.

n-i-p-i Superlattice Photoconductors

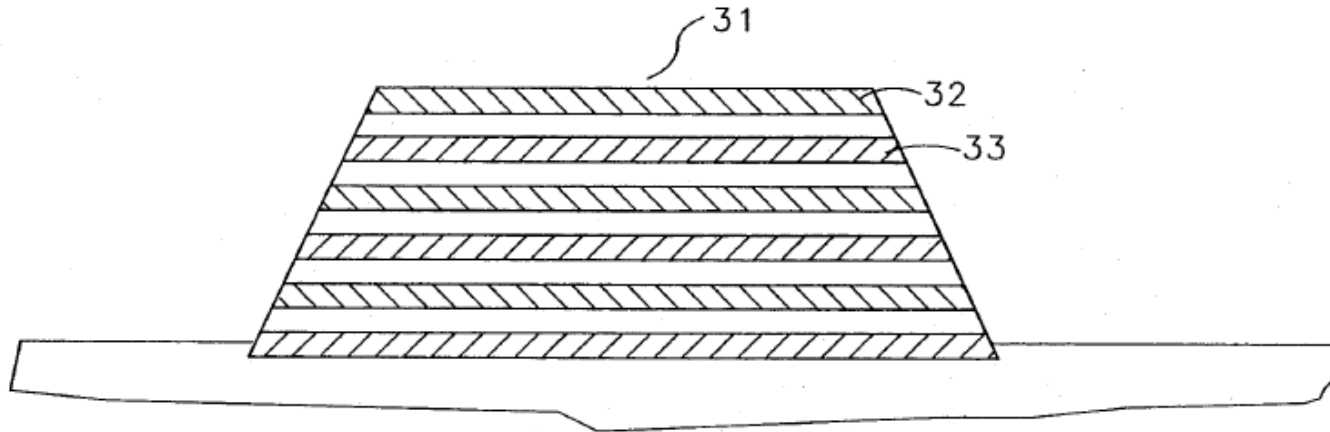


FIG 3A

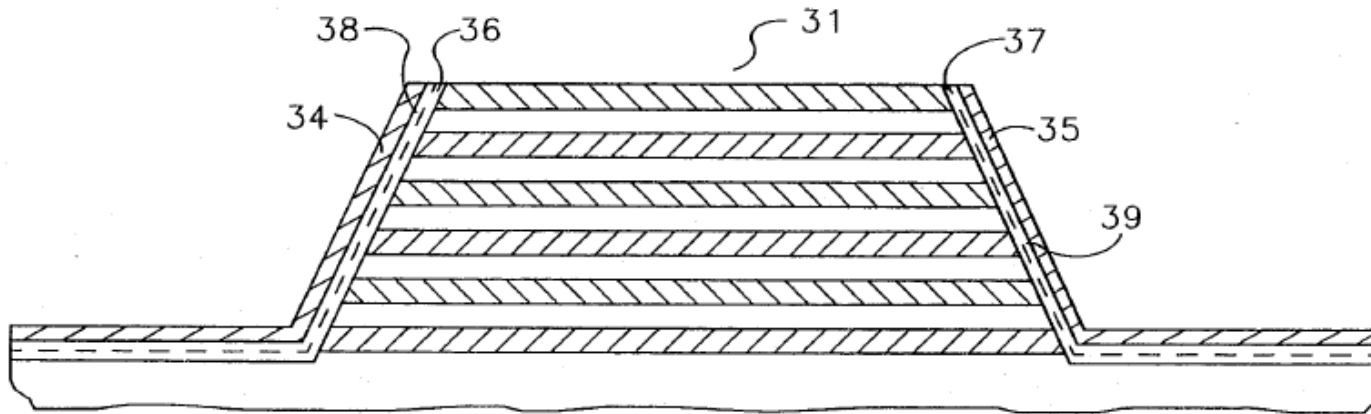


FIG 3B

United States Patent [19]
Doehler et al.

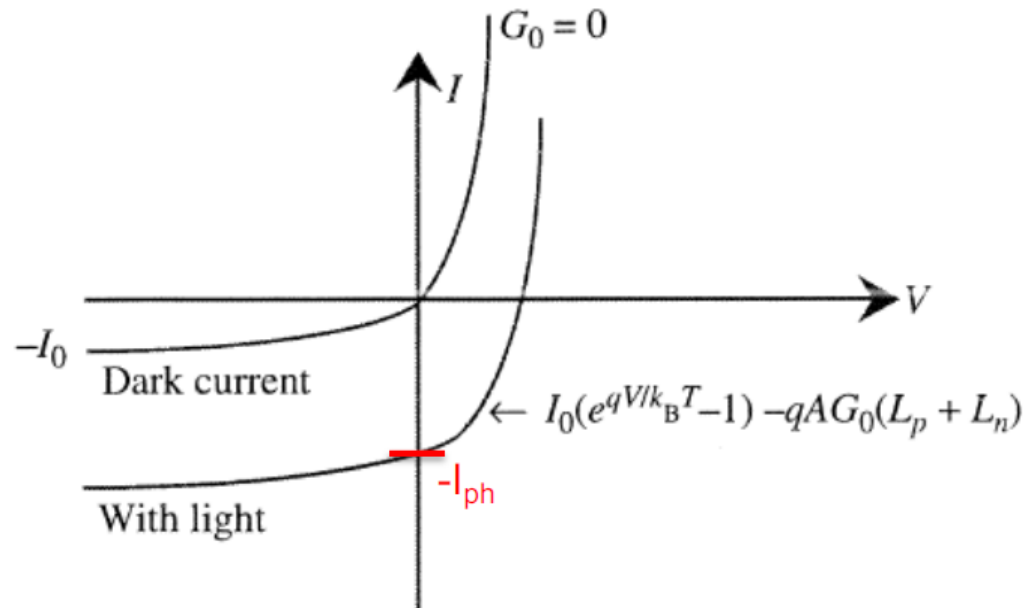
[11] **Patent Number:** 4,839,714
[45] **Date of Patent:** Jun. 13, 1989

Junction Diodes

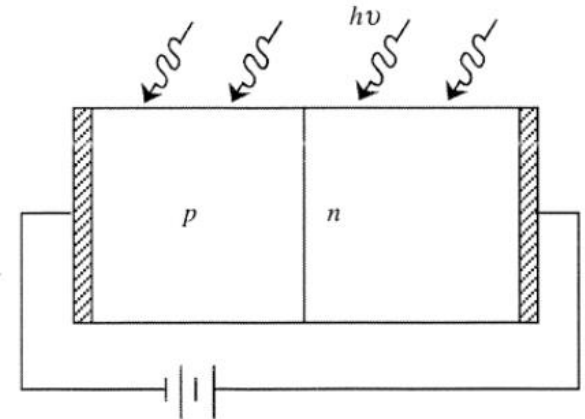
p-n Photodiode

Limitations

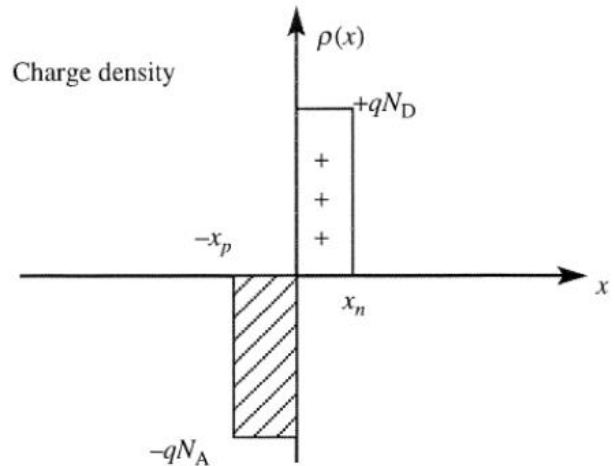
- Small optical absorption (within one diffusion length of depletion layer)
- Slow diffusion process
- High junction capacitance



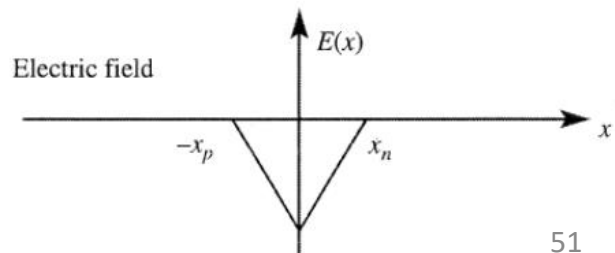
(a) A $p-n$ junction photodiode



(b) Charge density



(c) Electric field

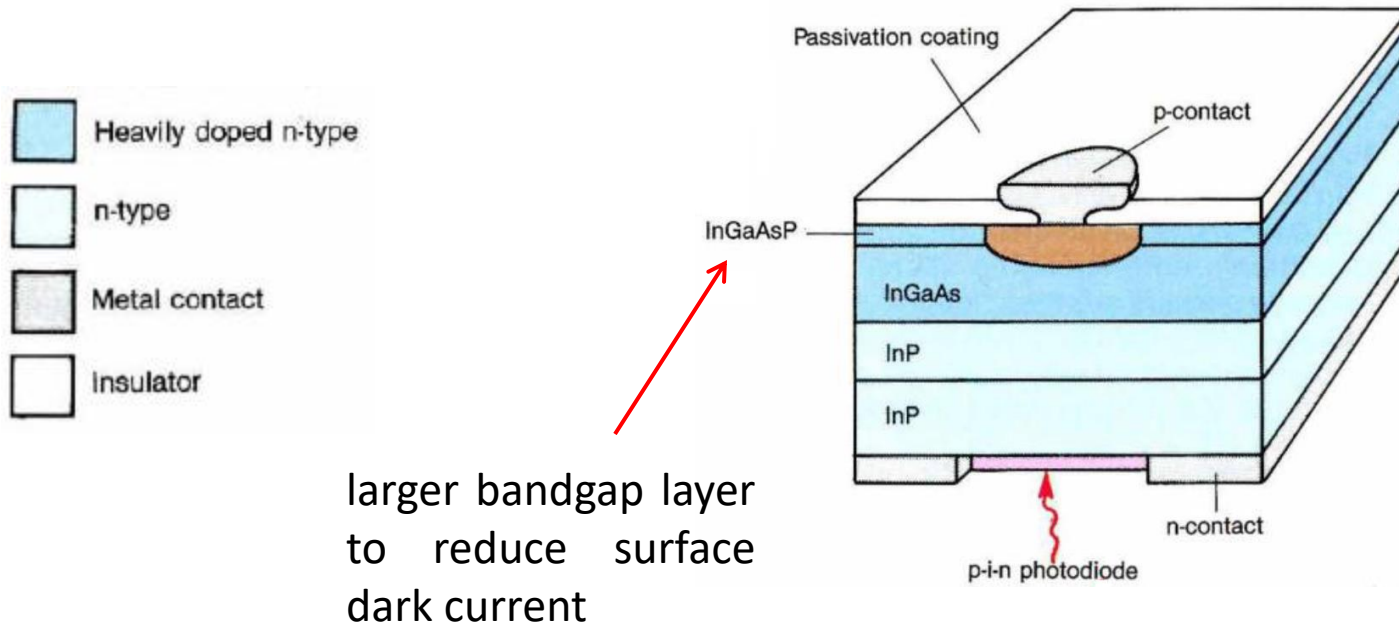


Junction Diodes

p-i-n Photodiode

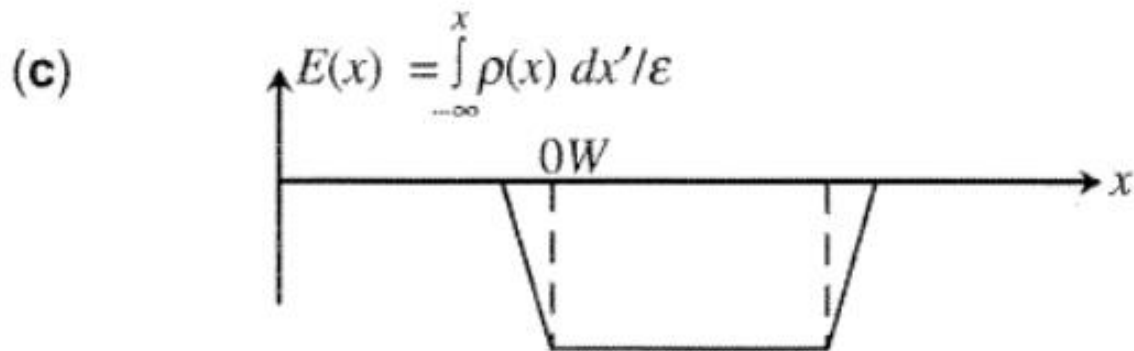
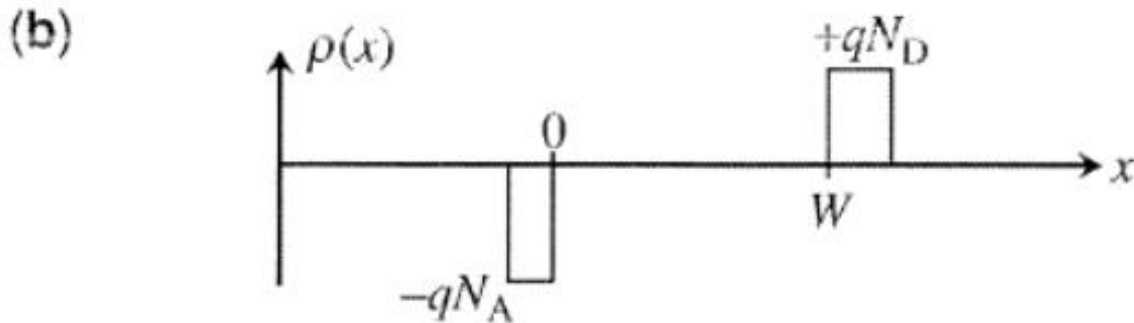
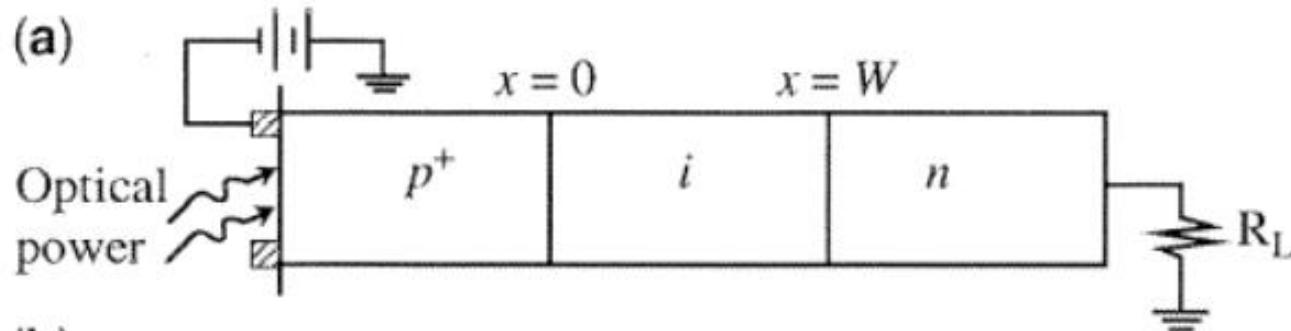
To overcome the issues with *p-n* photodiodes, an intrinsic (or lightly doped) region is inserted to increase the absorption volume.

This results in higher external efficiency and lower noise.



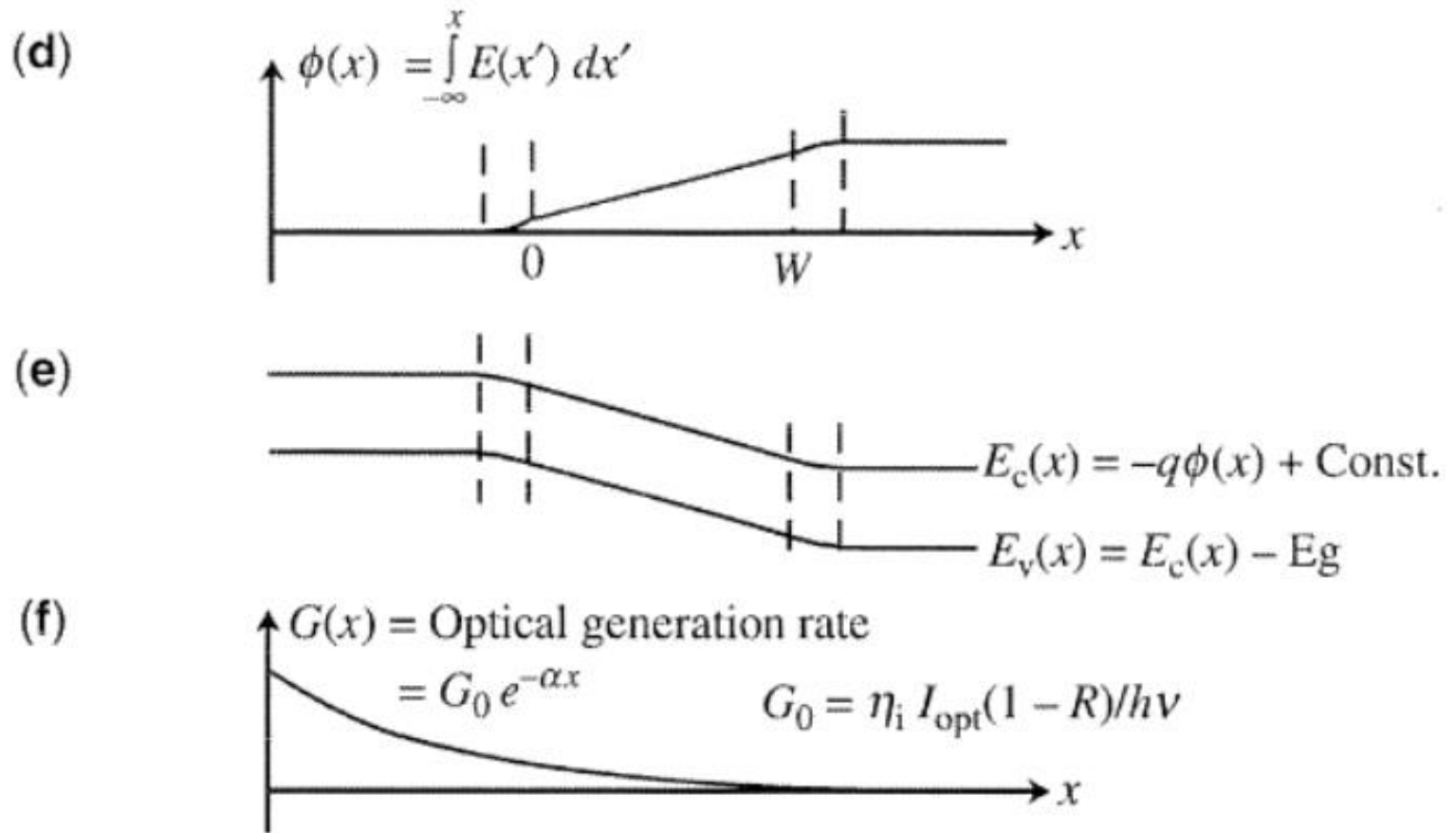
Junction Diodes

p-i-n Photodiode



Junction Diodes

p-i-n Photodiode



Junction Diodes

p-i-n Photodiode

Devices can be made smaller. The junction area can be matched to the size of the incident light beam.

The coupling efficiency of the light to the diode can be near unity, i.e., almost one electron-hole pair collected per incident photon.

There is no gain mechanism in *p-i-n* photodiodes. The ultimate bandwidth is limited to the time necessary to collect the charges. This is inversely proportional to the width of the depletion region and directly proportional to the velocity of the charge carriers in the region of high electric field (10^5 V/cm is a typical value).

Bandwidth of typical InGaAs *p-i-n* photodiode may exceed 10GHz and is typically limited by RC constant and external circuit,

Junction Diodes

p-i-n Photodiode

The principal source of noise is shot-noise in the depletion region of the reversed biased p-n junction, arising from small, randomly varying, thermally generated currents. Shot-noise is usually several orders of magnitude smaller than Johnson noise in photoconductors.

Therefore, p-i-n diodes are more sensitive devices than photoconductors.

Key points to create highly efficient p-i-n diodes:

- Illuminate the p-n junction through the substrate
- Achieve complete depletion within a thick absorbing layer (high purity of the intrinsic layer is desirable)
- Low-voltage operation to minimize noisy background current (originating, for instance, from tunneling).

Noise Equivalent Power and Detectivity

The noise equivalent power (NEP) is defined as the amount of optical power that yields a signal-to-noise ratio of one when the detector bandwidth is 1 Hz.

The specific detectivity (D^*) is a figure of merit used to characterize performance taking into account how the detector's noise increases in proportion to the square root of detector area and detector bandwidth:

$$D^* = \frac{\sqrt{A\Delta f}}{NEP} \text{ cm (Hz)}^{1/2} / W$$

The specific detectivity allows one to compare the intrinsic properties of two detectors. Higher values indicate higher sensitivity.

Examples

PbSe Photoconductor: 1.5 - 4.8 μm



[Zoom](#)

- ▶ Good Performance for 1.5 - 4.8 μm Range
- ▶ For Detection of CW Light We Recommend an [Optical Chopper](#)
- ▶ Also Comes as a Packaged, Amplified Detector, the [PDA20H](#)

Item #	Info	Wavelength Range	Active Area	Package Type	Rise Time ^b	Peak Wavelength	Peak Sensitivity ^c	Specific Detectivity ^d	Dark Resistance	Compatible Sockets
FDPSE2X2	Info	1.5 - 4.8 μm	4 mm ²	TO-5	10 μs	4 μm (Typ.)	3.0 x 10 ³ V/W	2.5 x 10 ⁹ cm \cdot Hz ^{1/2} /W (Typ.)	0.1 - 3.0 M Ω	STO5S STO5P

- All measurements performed with a 50 Ω load unless stated otherwise
- Rise time is measured from 0 - 63% of final value
- Measured at peak wavelength, chopping frequency of 600Hz, and bias voltage of 15 V, $R_{\text{DARK}} = R_{\text{LOAD}}$
- Measured at peak wavelength and a chopping frequency of 600 Hz

Based on your currency / country selection, your order will ship from Newton, New Jersey

+1	Qty	Docs	Part Number - Universal/Imperial	Price	Available / Ships
	<input type="text"/>		FDPSE2X2 PbSe Photoconductor, 2 mm x 2 mm Active Area, 10 μs Rise Time, 1.5 - 4.8 μm	\$210.00	✓ Today

$$NEP = \frac{\sqrt{A\Delta f}}{D^*} = \frac{2\text{mm}\sqrt{\Delta f}}{2.5 \times 10^9 \text{ cm} \cdot \text{Hz}^{1/2} / \text{W}}$$

$$\Delta f \approx \frac{0.35}{t_r} = 35\text{kHz} = 35000\text{Hz} \text{ so}$$

$$NEP \approx \frac{0.2\text{cm}\sqrt{35000} \cdot \text{Hz}^{1/2}}{2.5 \times 10^9 \text{ cm} \cdot \text{Hz}^{1/2} / \text{W}} = 15\text{nW}$$

Examples

PbS Photoconductor: 1.0 - 2.9 μm



[Zoom](#)

- ▶ Good Performance for 1.0 - 2.9 μm Range
- ▶ For Detection of CW Light We Recommend an [Optical Chopper](#)
- ▶ Also Comes as a Packaged, Amplified Detector, the [PDA30G](#)

Item #	Info	Wavelength Range	Active Area	Package Type	Rise Time ^b	Peak Wavelength	Peak Sensitivity ^c	Specific Detectivity ^d	Dark Resistance	Compatible Sockets
FDPS3X3	i	1.0 - 2.9 μm	9 mm ²	TO-5	200 μs	2.2 μm (Typ.)	2 x 10 ⁴ V/W (Min) 5.0 x 10 ⁴ V/W (Typ.)	1 x 10 ¹¹ cm ² Hz ^{1/2} /W	0.25 - 2.5 M Ω	STO5S STO5P

- All measurements performed with a 50 Ω load unless stated otherwise
- Rise time is measured from 0 - 63% of final value
- Measured at peak wavelength, chopping frequency of 600 Hz, and bias voltage of 15 V, $R_{\text{DARK}} = R_{\text{LOAD}}$
- Measured at peak wavelength and chopping frequency of 600 Hz

Based on your currency / country selection, your order will ship from Newton, New Jersey

+1	Qty	Docs	Part Number - Universal/Imperial	Price	Available / Ships
+	<input type="text"/>		FDPS3X3 PbS Photoconductor, 3 mm x 3 mm Active Area, 200 μs Rise Time, 1.0 - 2.9 μm	\$177.50	✓ Today

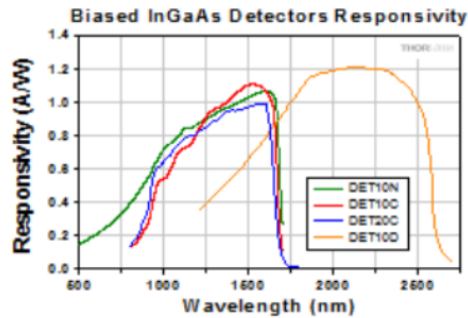
$$NEP = \frac{\sqrt{A\Delta f}}{D^*} = \frac{3\text{mm}\sqrt{\Delta f}}{10^{11} \text{cm} \cdot \text{Hz}^{1/2} / \text{W}}$$

$$\Delta f \approx \frac{0.35}{t_r} = 1.75\text{kHz} = 1750\text{Hz} \text{ so}$$

$$NEP \approx \frac{0.3\text{cm}\sqrt{1750} \cdot \text{Hz}^{1/2}}{10^{11} \text{cm} \cdot \text{Hz}^{1/2} / \text{W}} = 125\text{pW}$$

Examples

Biased InGaAs Detectors: 500 - 2600 nm



[Click to Enlarge](#)
Click [Here](#) for Raw Data

Item #	Active Area	Wavelength Range	Rise Time	NEP	Dark Current	Junction Capacitance ^a	Bias Voltage
DET10N	0.8 mm ² (Ø1 mm)	500 - 1700 nm	5 ns	0.2 x 10 ⁻¹² W/Hz ^{1/2}	1.5 nA (Typ.) 10 nA (Max)	50 pF	5.0 V
DET10C	0.8 mm ² (Ø1.0 mm)	700 - 1800 nm	10 ns	2.54 x 10 ⁻¹⁴ W/Hz ^{1/2}	1 nA (Typ.) 25 nA (Max)	40 pF	5 V
DET20C	3.1 mm ² (Ø2.0 mm)	800 - 1800 nm	25 ns	0.03 x 10 ⁻¹² W/Hz ^{1/2}	55 nA (Typ.) 200 nA (Max)	100 pF	1.8 V
DET10D	0.8 mm ² (Ø1.0 mm)	1200 - 2600 nm	25 ns	2 x 10 ⁻¹² W/Hz ^{1/2}	15 µA (Typ.) 75 µA (Max)	175 pF	1.8 V

a. Typical values, R_L = 50 Ohm

Based on your currency / country selection, your order will ship from Newton, New Jersey

+1	Qty	Docs	Part Number - Universal/Imperial	Price	Available / Ships
	<input type="text"/>		DET10N InGaAs Detector, 500-1700 nm, 5 ns Rise Time, 0.8 mm ²	\$478.69	✓ Today
	<input type="text"/>		DET10C InGaAs Detector, 700-1800 nm, 10 ns Rise Time, 0.8 mm ²	\$282.23	✓ Today
	<input type="text"/>		DET20C InGaAs Detector, 800-1800 nm, 25 ns Rise Time, 3.14 mm ²	\$386.58	✓ Today
	<input type="text"/>		DET10D InGaAs Detector, 1200-2600 nm, 25 ns Rise Time, 0.8 mm ²	\$478.69	✓ Today

$$D^* = \frac{\sqrt{A\Delta f}}{NEP} = \frac{0.9\text{mm}\sqrt{\Delta f}}{2.5 \times 10^{-14} \text{ W}}$$

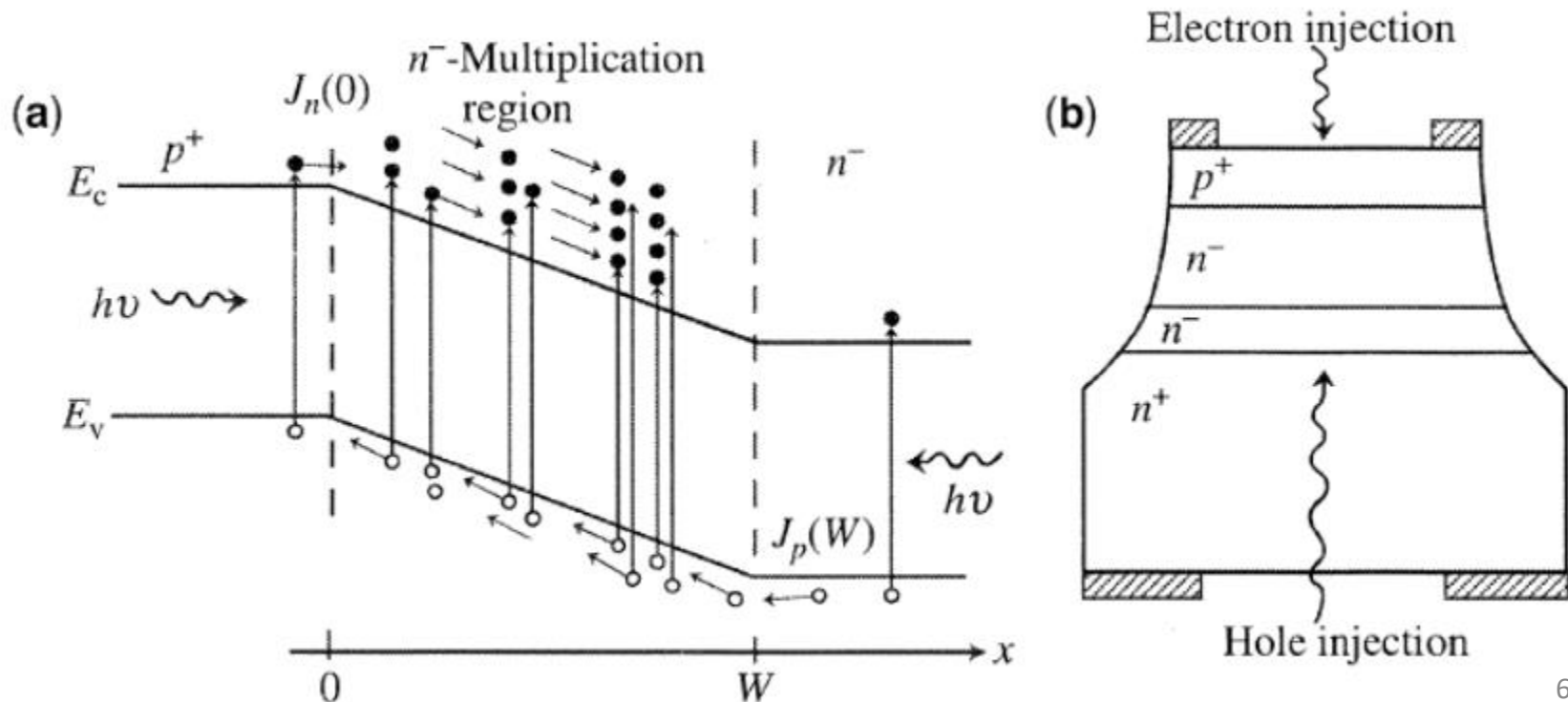
$$\Delta f \approx \frac{0.35}{t_r} = 35\text{MHz} = 3.5 \times 10^7 \text{ Hz}$$

$$D^* \approx \frac{0.09\text{cm}\sqrt{3.5 \times 10^7 \text{ Hz}}}{2.5 \times 10^{-14} \text{ W}} = 2.13 \times 10^{16} \text{ cm} \cdot \text{Hz}^{1/2} / \text{W}$$

Avalanche Photodiodes (APDs)

Typical Applications:

- Long-haul telecommunications
- Scientific & Medical Instrumentation
- Photon Counting
- Distance Measurement / Range Finding



Avalanche Photodiodes (APDs)

- The absorption of photons within the multiplication region creates electron-hole pairs.
- Within this region, the electrons and holes are accelerated by the electric field and produce more electron-hole pairs through impact ionization.
- To minimize noise, it's best if only one type of carrier ionizes pairs.

Ionization coefficient is the number of e-h pairs created per unit distance per incident electron (cm⁻¹)

α_n = electron ionization coefficient

β_p = hole ionization coefficient

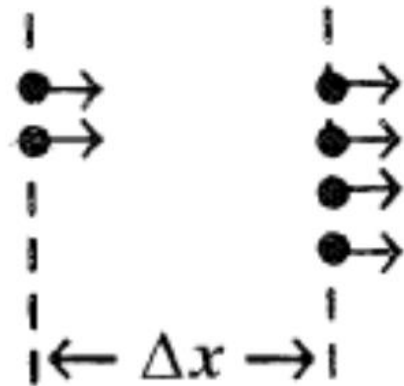
$$\alpha_n(E) = \alpha_0 e^{-C_n/E}$$

$$\beta_p(E) = \beta_0 e^{-C_p/E}$$

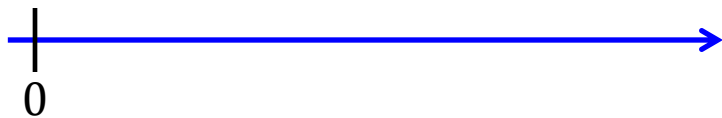
Simplified Analysis: Electron Multiplication

$$J_n(x + \Delta x) = J_n(x) + \alpha_n \Delta x J_n(x) \quad \longrightarrow \quad \frac{d}{dx} J_n(x) = \alpha_n J_n(x) \quad \text{differential form}$$

$$J_n(x) \quad J_n(x + \Delta x)$$



$$x \quad x + \Delta x$$



General case: $\alpha_n = \alpha_n(x)$

$$J_n(x) = J_n(0) e^{\int_0^x \alpha_n(x') dx'}$$

Multiplication factor

$$M_n = \frac{J_n(W)}{J_n(0)} = e^{\int_0^W \alpha_n(x') dx'}$$

For uniform α $J_n(x) = J_n(0) e^{\alpha_n x}$

$$M_n = e^{\alpha_n W}$$

Simplified Analysis: Hole Multiplication

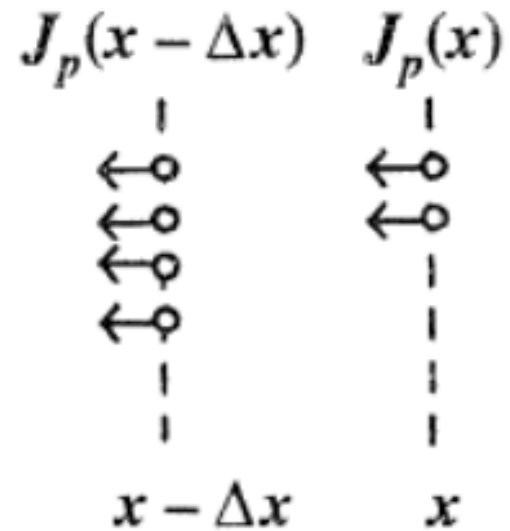
$$J_p(x - \Delta x) = J_p(x) + \beta_p \Delta x J_p(x) \quad \longrightarrow \quad -\frac{d}{dx} J_p(x) = \beta_p J_p(x)$$

General case: $\beta_p = \beta_p(x)$

$$J_p(x) = J_p(W) e^{\int_0^x \beta_p(x') dx'}$$

Multiplication factor

$$M_p = \frac{J_p(0)}{J_p(W)} = e^{\int_0^W \beta_p(x') dx'}$$



For uniform β

$$J_p(x) = J_p(W) e^{\beta_p(W-x)}$$

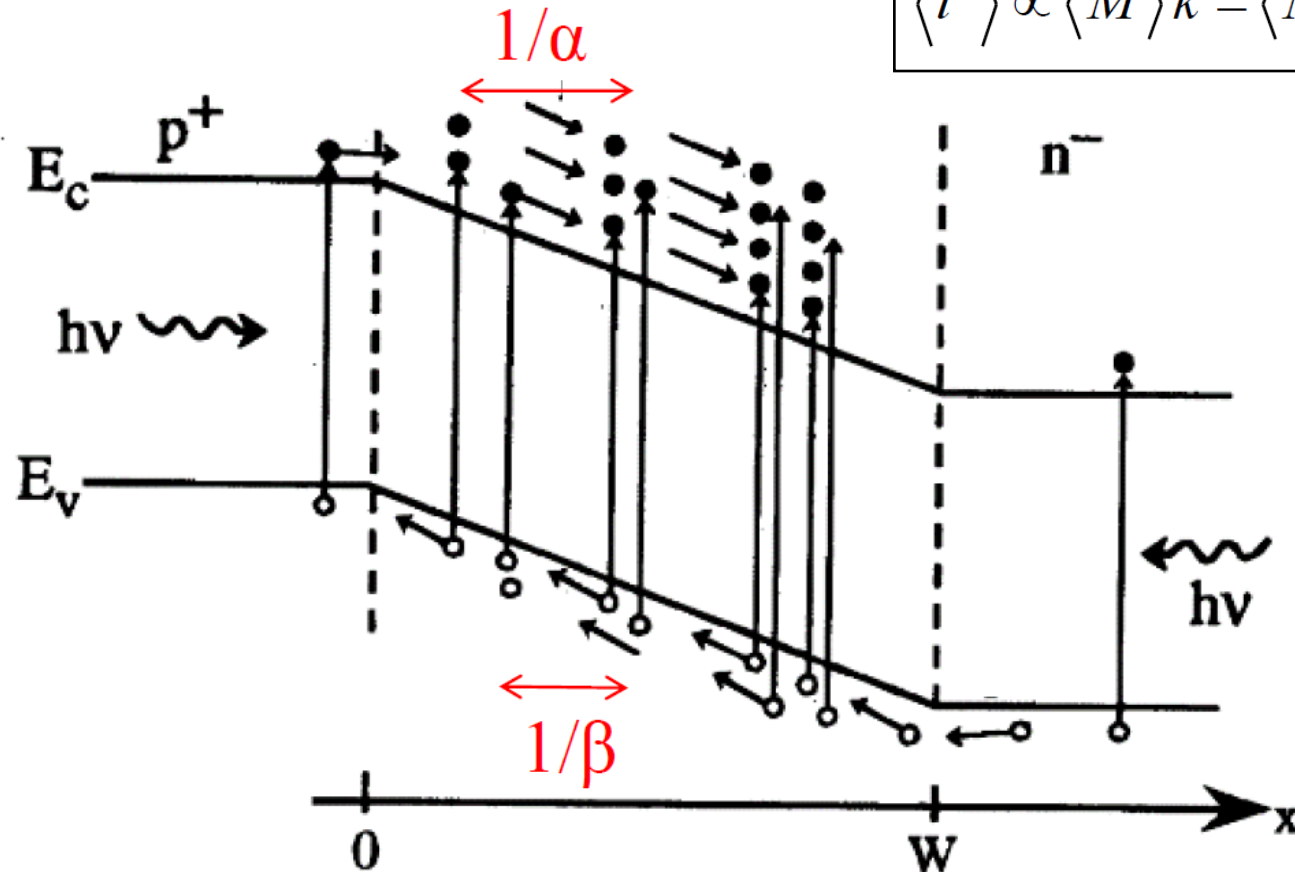
$$M_p = e^{\beta_p W}$$

Much more involved model for coupled e-h ionization...
(Section 15.4 of Chuang's book)

Noise in APDs

- Field accelerates carriers (kinetic energy $> E_g$)
- Transfers energy to generate electron-hole pairs \rightarrow **Gain**
- Stochastic nature of impact ionization multiplication \rightarrow **Noise**
- Limited by the ratio $k = \beta/\alpha$

$$\langle i^2 \rangle \propto \langle M \rangle k = \langle M \rangle \beta / \alpha$$



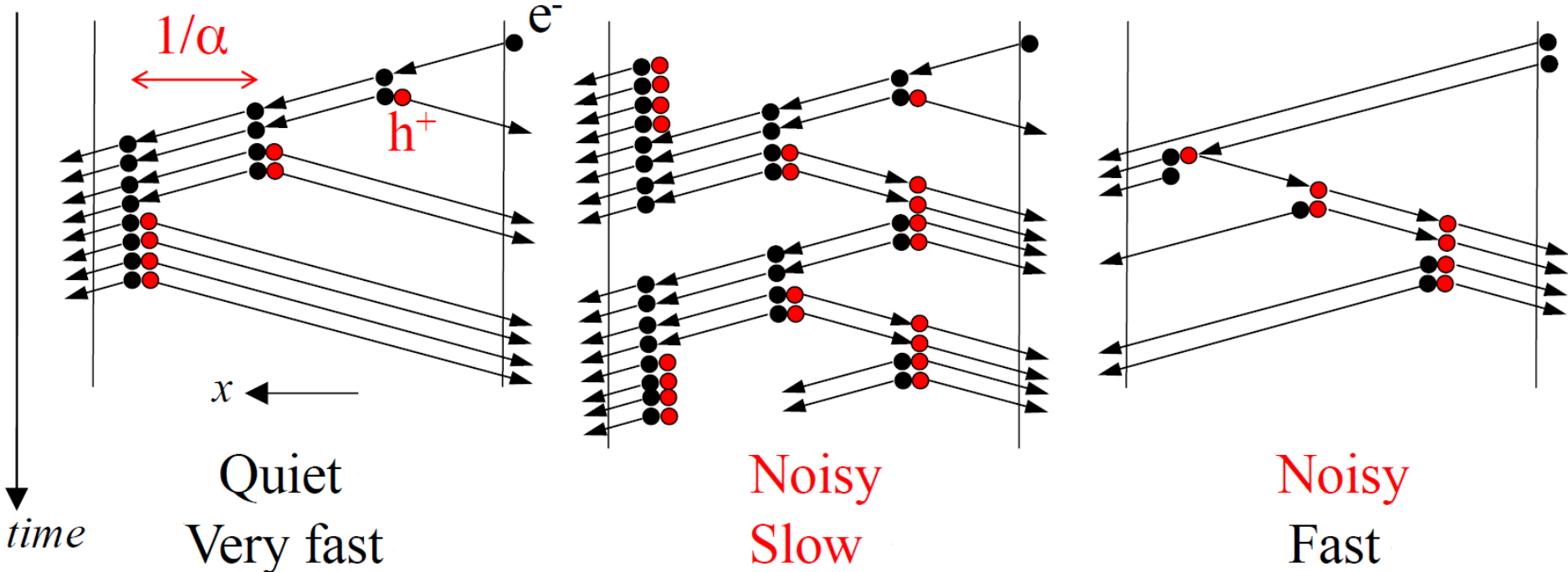
Noise in APDs

Limited by the ratio $k = \beta/\alpha$

$$k = \beta/\alpha \ll 1$$

$$k = \alpha/\beta \approx 1$$

$$k = \beta/\alpha \gg 1$$



Noise in APDs

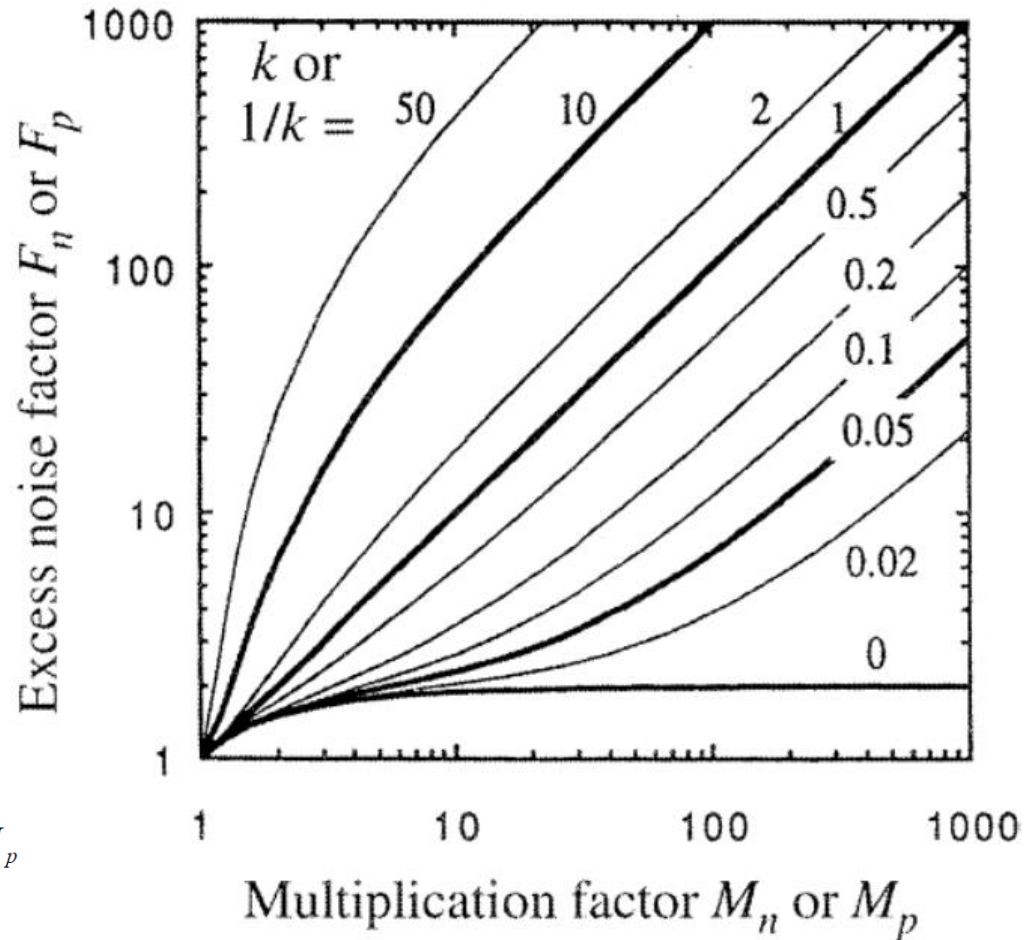
- Secondary random processes further increase noise

Excess Noise :

$$F(M) = \frac{\langle M^2 \rangle}{\langle M \rangle^2}$$

$$F_n = \frac{\beta_p}{\alpha_n} \langle M_n \rangle + \left(1 - \frac{\beta_p}{\alpha_n}\right) \left(2 - \frac{1}{\langle M_n \rangle}\right)$$

$$F_p = \frac{\alpha_n}{\beta_p} \langle M_p \rangle + \left(1 - \frac{\alpha_n}{\beta_p}\right) \left(2 - \frac{1}{\langle M_p \rangle}\right)$$



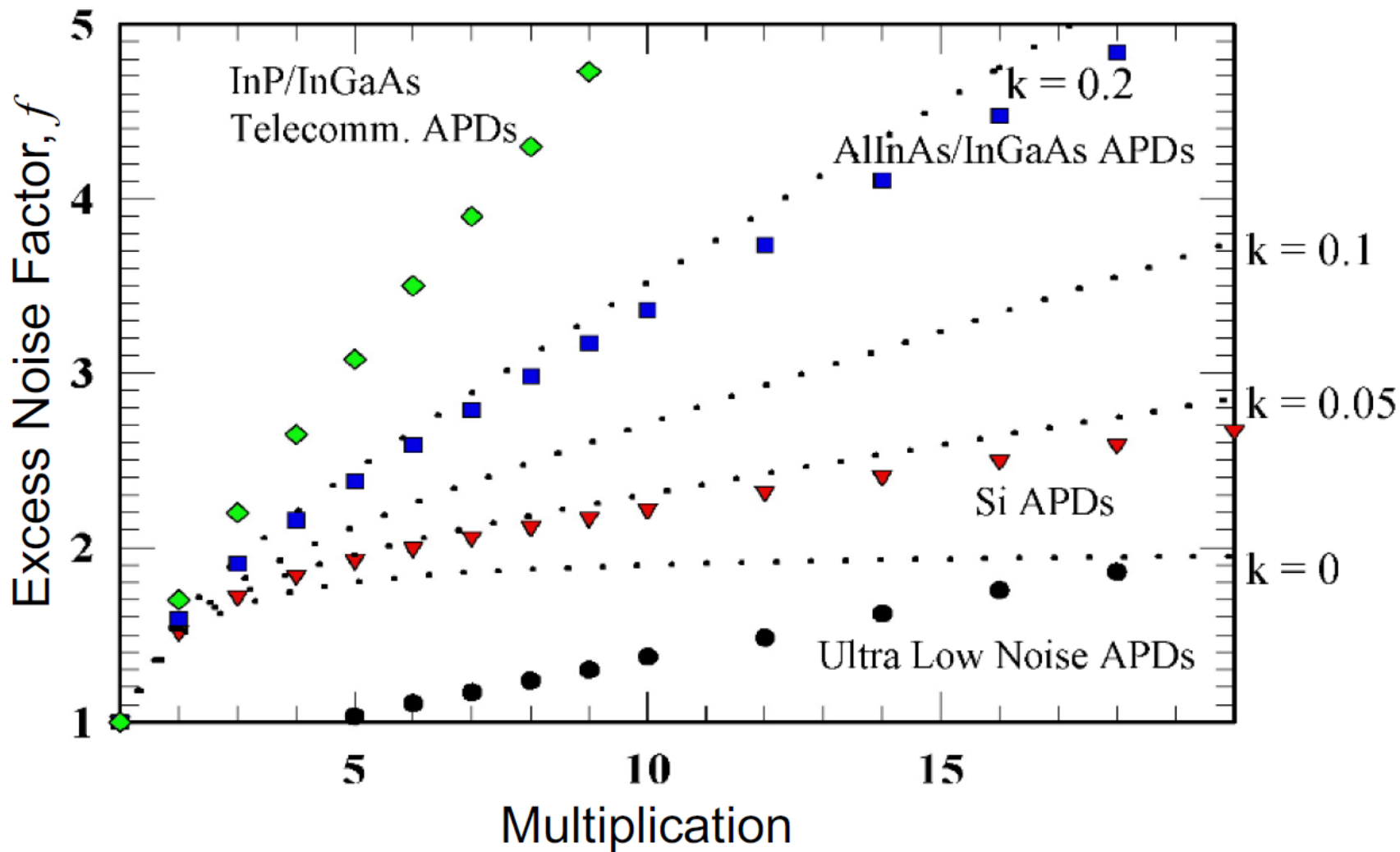
Other Noise Sources in APDs :

Multiplication (Gain) Noise: $\langle i_M^2 \rangle = 2q \langle M \rangle I_p F(M) I_p$

Shot Noise: $\langle i_S^2 \rangle = 2q (I_p + I_B + I_D) \langle M \rangle^2 F(M) B$

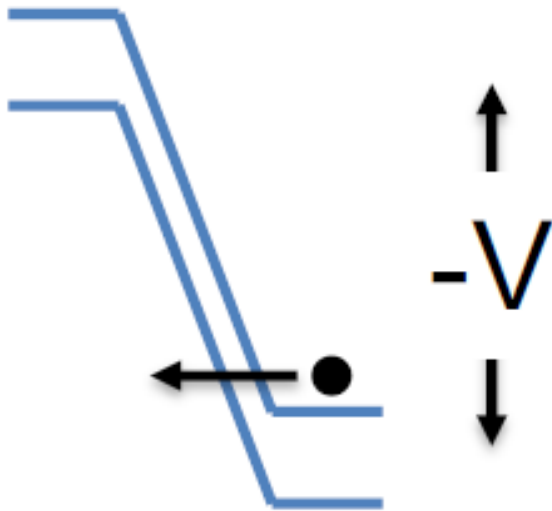
Thermal Noise: $\langle i_S^2 \rangle = \frac{4k_B T}{R_{eq}} B$

Excess Noise in APDs

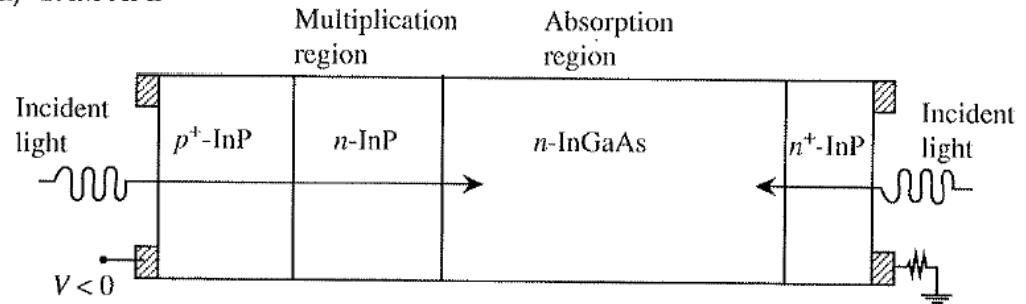


Separate Absorption-Multiplication APDs

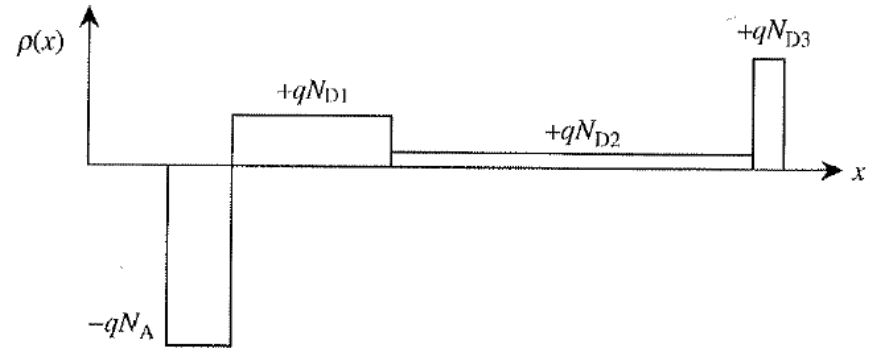
Includes separate regions for absorption multiplication to reduce dark current at high reverse bias, especially from carriers tunneling across the bandgap.



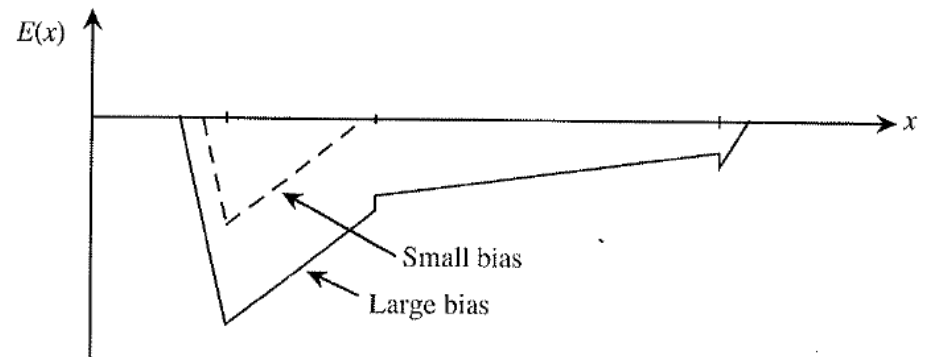
(a) SAM APD



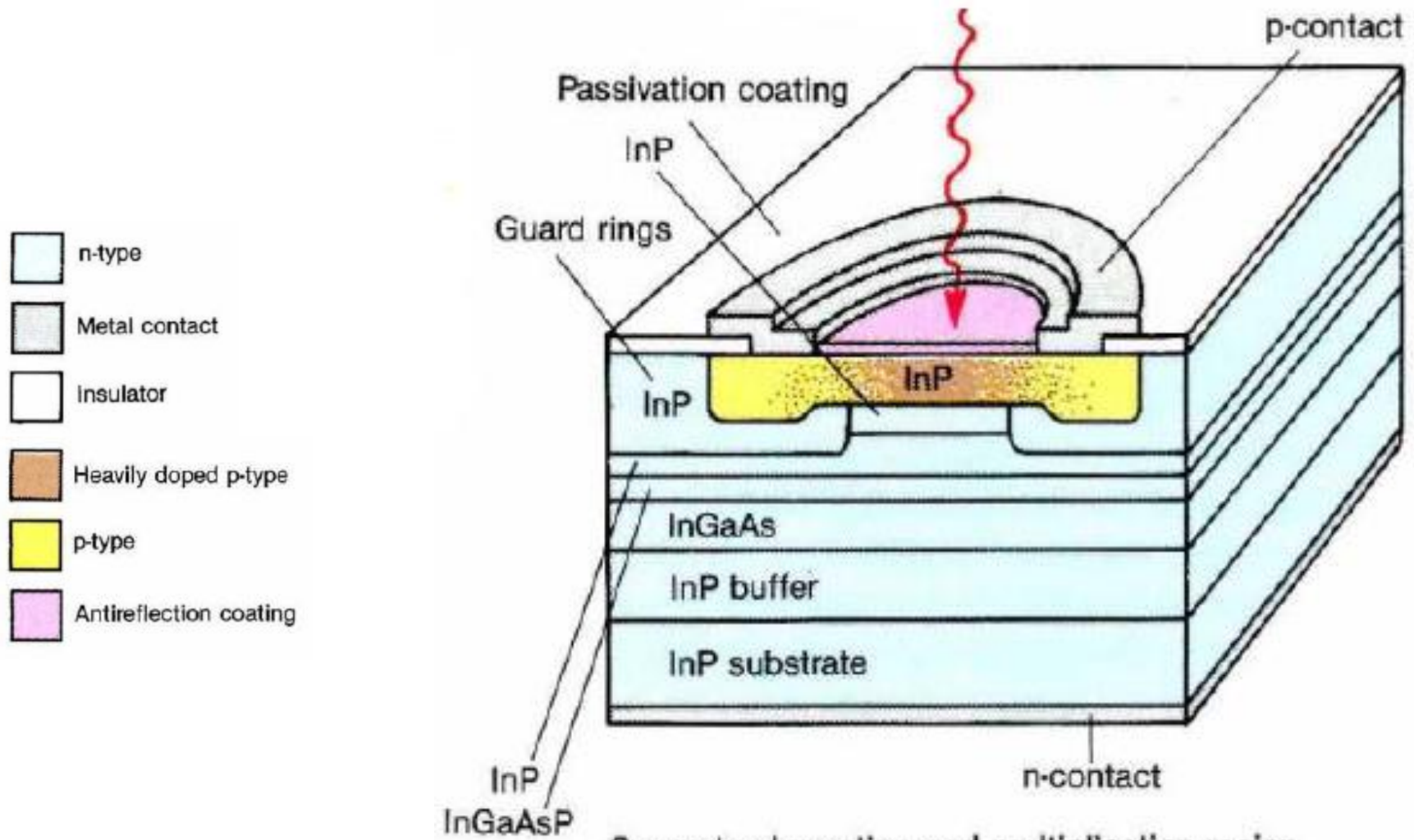
(b) Charge distribution



(c) Electric field profile $\mathbf{E} = \hat{x} E(x)$

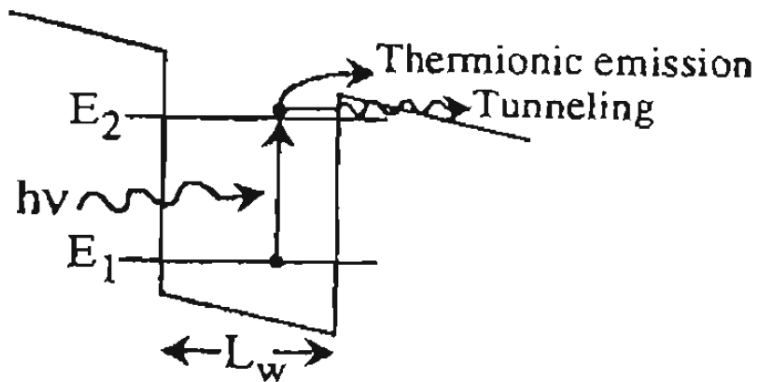
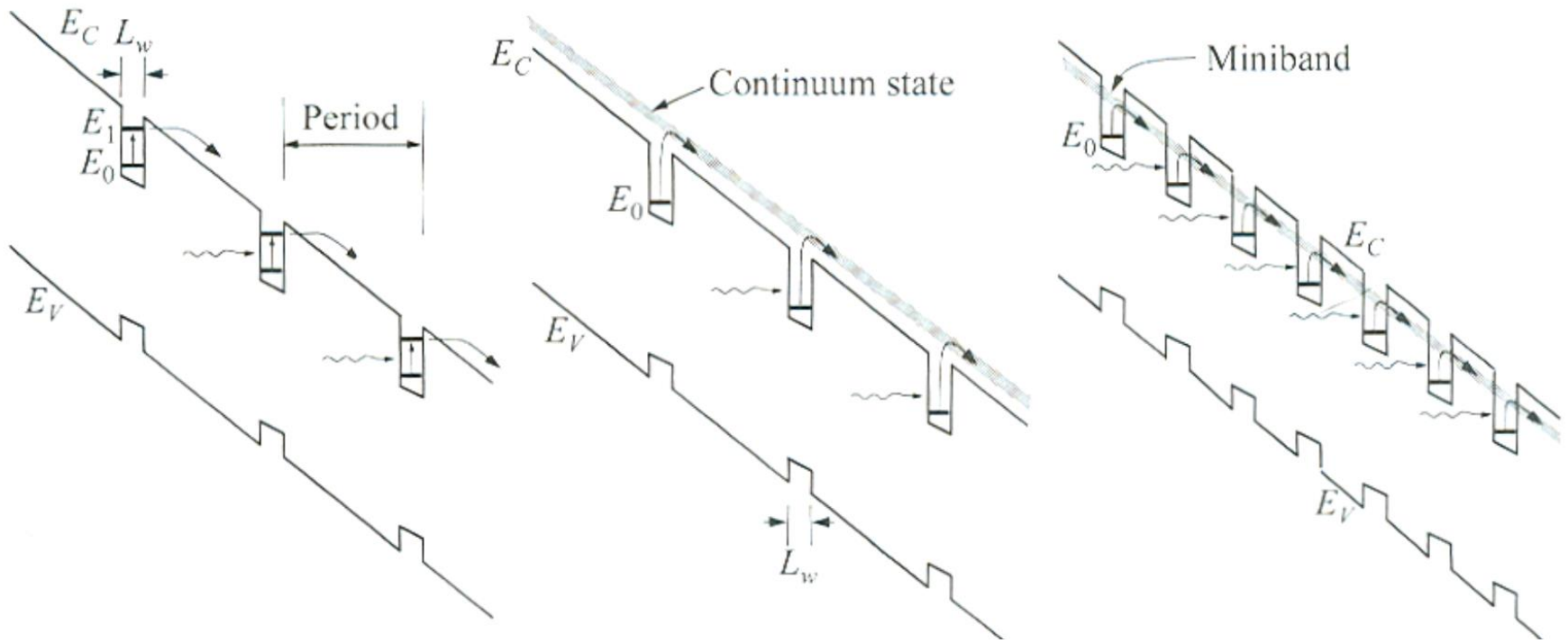


Separate Absorption-Multiplication APDs

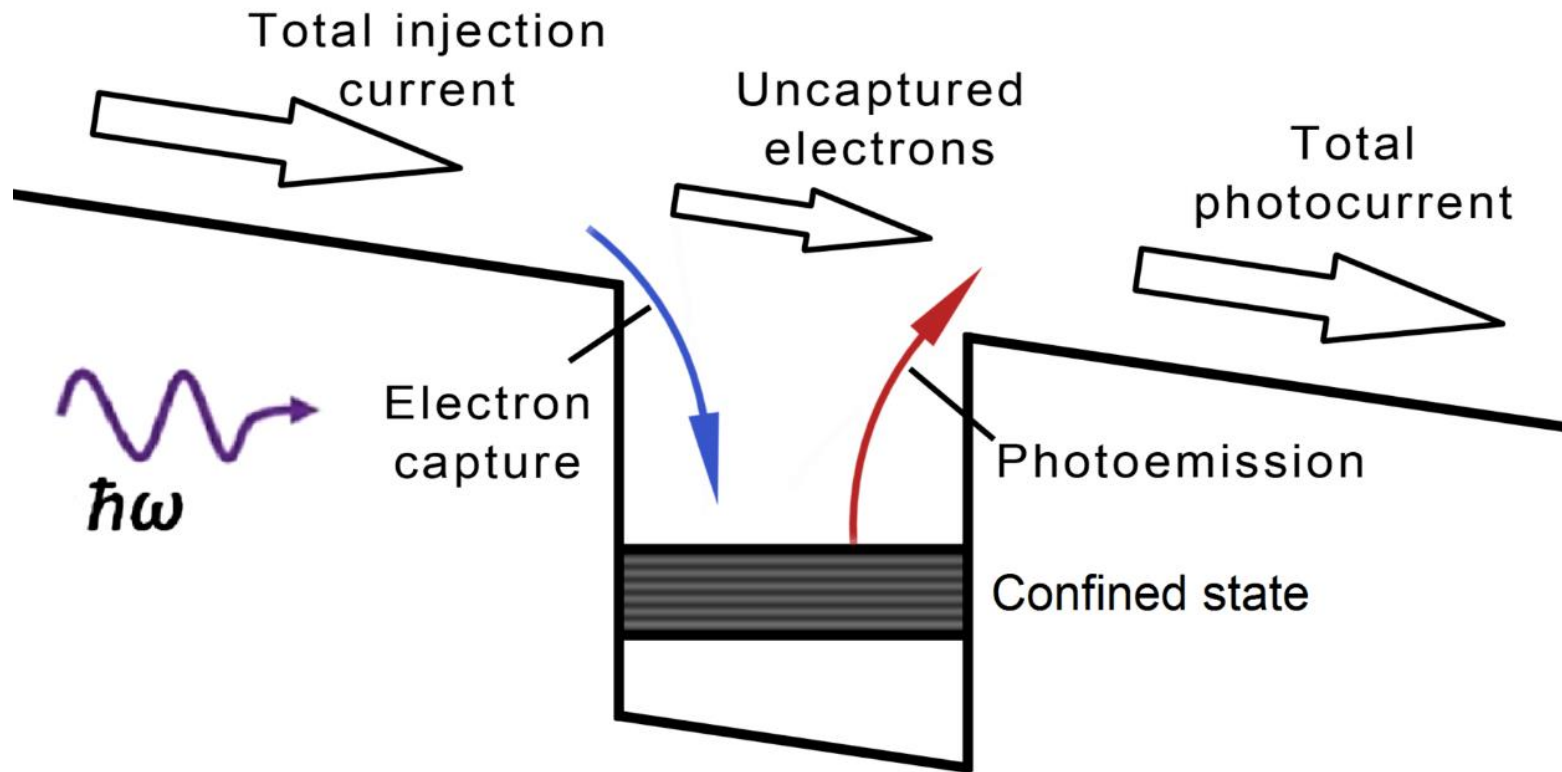


Separate absorption and multiplication region avalanche photodiode (SAM-APD)

Quantum Well Infrared Photodetectors (QWIPs)



Quantum Well Infrared Photodetectors (QWIPs)



Photoconductive gain

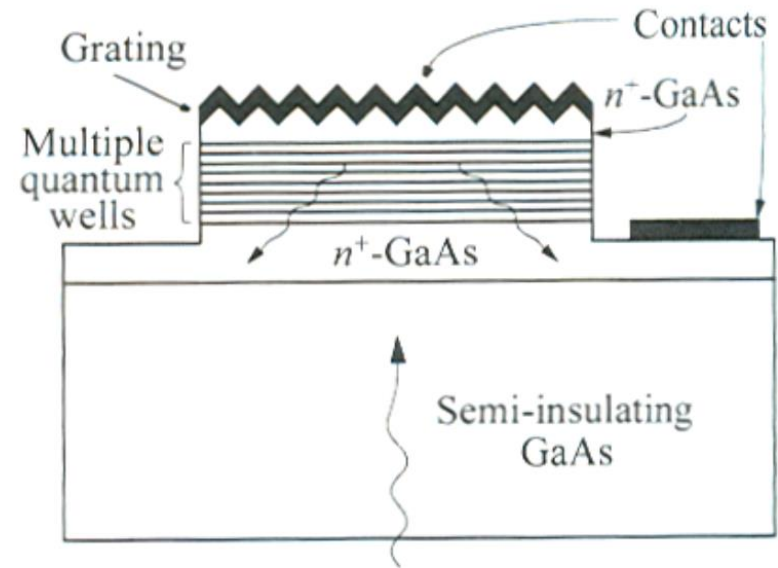
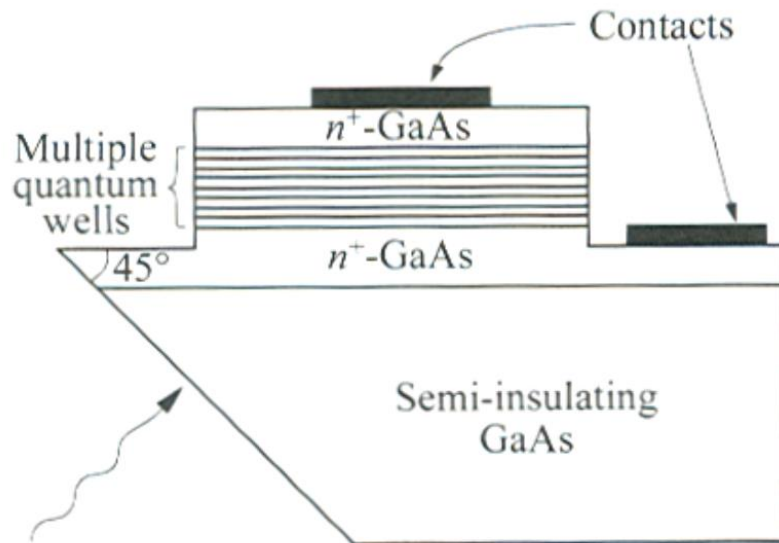
$$g_{ph} = \frac{p_e}{N p_c}$$

← escape probability

← capture probability

quantum wells

Quantum Well Infrared Photodetectors (QWIPs)



Good solution for 2D imaging arrays

Reading Assignments:

- Section 12.1 of Chuang's book
- Chapter 8 of Chuang's book
- Chapter 13 of Chuang's book

- Chapter 15 of Chuang's book

FROM THE BUSINESS WORLD

CASE STUDY

Wave propagation speed is very relevant for our globally interconnected world.

<https://www.scientificamerican.com/article/an-internet-cable-will-soon-cross-the-arctic-circle/>
Scientific American, June 2016



The underwater fiber-optic cable would trace the shortest path between Europe and Asia

London-Tokyo via Northwest passage

$$L_1 \approx 9,600 \text{ miles} = 9,600 \times 1,609 = 15,446,400 \text{ m}$$

Assume dielectric constant of fiber optic glass core

$$\epsilon_r = 2.25$$

Propagation along the axis of the fiber (exact c)

$$v_g = \frac{c}{\sqrt{\epsilon_r}} = \frac{299,792,458}{\sqrt{2.25}} = 199,861,638.7 \frac{\text{m}}{\text{s}}$$

$$t_{LT1} = \frac{L}{v_g} = \frac{15,446,400}{199,861,638.7} = 0.0772855\text{s}$$

With approximate $c = 3 \times 10^8 \text{ m/s}$

$$t_{LT1} = \frac{L}{v_g} \approx \frac{15,446,400}{2 \times 10^8} = 0.077232\text{s}$$

time is underestimated by $\approx 53 \mu\text{s}$

London-Tokyo via New York – San Francisco

$$L_2 \approx 11,500 \text{ miles} = 11,500 \times 1,609 = 18,503,500 \text{ m}$$

Assume again

$$v_g = 199,861,638.7 \frac{\text{m}}{\text{s}}$$

Propagation along the axis of the fiber

$$t_{LT1} = \frac{L}{v_g} = \frac{15,446,400}{199,861,638.7} = 0.0772855 \text{ s}$$

$$t_{LT2} = \frac{L}{v_g} \approx \frac{18,503,500}{199,861,638.7} = 0.0925816 \text{ s}$$

$$\Delta t \approx 15.3 \text{ ms}$$

London-Tokyo via satellite?

Signals move faster in air/vacuum than in fiber optic glass, but a geosynchronous satellite is at an altitude

$$H = 22,236 \text{ miles} = 35,786 \text{ km}$$

(≈ 4 times the height of Mt. Everest and $\approx 89\%$ length of the equator)

The speed of EM waves in air is $v_g \approx 3 \times 10^8$ instead of $v_g \approx 2 \times 10^8$ in glass but the link distance to be covered would be at least more than five times the shortest one between London and Tokyo via the Northwest passage.

Nonetheless, for purposes other than trading, the additional delay may be quite reasonable and business entities are indeed exploring an expansion of satellite links:

<https://www.businesswire.com/news/home/20210513005383/en/SoftBank-Corp.-and-OneWeb-Agree-on-Collaboration-Towards-Satellite-Communication-Service-Business-Deployment-in-Japan-and-Global-Markets>

Processing time

One also needs to add consideration on the delay involved with information processing using different technologies.

For instance: When a signal is regenerated in a long-haul communication link, what is the time-advantage of using optical amplifiers (e.g., erbium doped fiber) with respect to the more traditional repeater involving conversion from optical to electrical (photodetector) and then back to optical (laser).

Similarly, all optical signal de-multiplexing using integrated multimode interference coupler versus electronic processing of the signal packets.